

CHAPTER TWO

2. LITERATURE REVIEW: SOIL MOISTURE MEASUREMENT

Monitoring of volumetric soil moisture content in the field calls for a fast and accurate method, which allows repeated measurements through time. There are currently two approaches for measuring the spatial distribution and temporal variation of soil moisture content: (i) point measurements; and (ii) remote sensing. This chapter reviews these techniques. However, the reader is reminded that this chapter is a review of the current measurement techniques and their inference for soil moisture content, and that not all of these techniques will be used in the subsequent chapters. The remote sensing interpretation techniques that will be used in later chapters are the Integral Equation Model (section 2.4.5.2.2) and the Modified Integral Equation Model (section 2.4.5.3). The intention of this chapter is to give an overview of soil moisture measurement methodologies, and to highlight the essential characteristics of the point measurement and remote sensing measurement techniques, in relation to estimating the spatial and temporal variation of soil moisture profiles. This allows the development of a soil moisture profile estimation algorithm in later chapters, which will be applicable to the soil moisture measurements available. The review of soil moisture profile estimation techniques is provided in Chapter 3.

2.1 POINT MEASUREMENT OF SOIL MOISTURE PROFILES

It has long been recognised that reliable, robust and automated methods for the measurement of soil moisture content can be extremely useful, if not essential, in hydrologic, environmental and agricultural applications. Over the last 70 years, this recognition has fostered the investment of a considerable amount of ingenuity in developing such methods. The following sections review these methods.

2.1.1 THERMOGRAVIMETRIC METHOD

The standard method of measuring the volumetric moisture content of a soil sample is the thermogravimetric method (AS 1289.2.1.1-1992), which consists of oven drying at 105°C and relating the change in mass to the volume of the sample.

$$\theta = \frac{W_w}{W_d} \frac{\rho_b}{\rho_w} \quad (2.1)$$

where θ is the volumetric soil moisture content fraction, W_w is the weight of water contained in the voids of the moist soil, W_d is the weight of dry soil, ρ_b is the soil bulk density (from collecting a known volume of soil), and ρ_w is the density of water.

The advantages of this method are that it is inexpensive and soil moisture is easily calculated. However, it is time consuming, difficult to obtain representative samples and destructive. Hence, this method cannot be used for repetitive measurements at exactly the same location (Roth *et al.*, 1990).

This method is prone to large errors due to sampling, transporting, handling and repeated weighing. In addition, soils with organic matter may exhibit a mass loss during oven drying due to oxidation and decomposition of the organic matter, while some clays will retain appreciable amounts of adsorbed water. Measurement errors may be reduced by increasing the size and number of samples (Zegelin, 1996).

2.1.2 NEUTRON SCATTERING METHOD

The neutron scattering method is an indirect way of determining soil moisture content. In this method, neutrons with high energy are emitted by a radioactive source into the soil and are slowed down by elastic collisions with nuclei of atoms. The energy loss is much greater for neutrons colliding with atoms of low atomic weight (primarily hydrogen in soils) than for collisions with heavier atoms. As a result, hydrogen can slow fast neutrons much more effectively than any other element present in the soil, thus giving a relationship with soil moisture

content. The number of slow neutrons returning to the detector per unit time are counted, and the soil moisture content estimated from a previously determined calibration curve of counts versus volumetric moisture content (Wilson, 1971; Schmugge *et al.*, 1980; Zegelin, 1996). The sphere of influence or effective volume of measurement varies from a radius of less than 10 cm in a wet soil to 25 cm or more in a dry soil (Zegelin, 1996).

Calibration of the Neutron Moisture Meter (NMM) depends on the strength of the radioactive source, the nature of the detector, the geometry of the source and the detector in the probe (McCauley and Stone, 1972), the materials used to construct the probe, the size and composition of the access tube, and the physical and chemical properties of the soil (Wilson, 1971). Therefore, if an accurate moisture content determination is desired, the probe should be calibrated for each soil type (Wilson, 1971; Schmugge *et al.*, 1980; Zegelin, 1996). However, field calibration of the neutron probe is extremely difficult (Grimaldi *et al.*, 1994; Grismer *et al.*, 1995). Furthermore, electrical equipment can drift, requiring standards for periodic re-calibration (Schmugge *et al.*, 1980; Zegelin, 1996).

The advantages of this system are that average moisture contents can be determined with depth, measurements are insensitive to temperature, it can accommodate automatic reading, and temporal soil moisture content changes can be monitored at the same site. Apart from calibration, the major disadvantages are a poor depth resolution, limited measurements of soil moisture content near the soil surface, and the potential health risks from exposure to radioactive materials (Schmugge *et al.*, 1980; Zegelin, 1996).

2.1.3 GAMMA RAY ATTENUATION METHOD

The gamma ray attenuation method is a radiation technique that can be used to determine soil moisture content within a 1 to 2 cm soil layer. This method assumes that scattering and absorption of gamma rays are related to the density of the matter in their path and that the bulk density of soil remains relatively constant as the wet density changes with moisture content. Changes in wet density are measured by the gamma ray attenuation method and the soil moisture content

determined from this density change (Wilson, 1971; Schmugge *et al.*, 1980; Zegelin, 1996).

The advantages of this system are that it is non-destructive and that data can be obtained over very small vertical distances. Its disadvantages are that it is costly and difficult to use, and that extreme care must be taken to ensure that the radioactive source is not a health hazard (Schmugge *et al.*, 1980). Gamma ray scanners are generally only used in laboratory situations due to the cumbersome nature of the equipment (Zegelin, 1996).

2.1.4 SOIL ELECTRICAL CONDUCTIVITY METHOD

Soil electrical conductivity is a function of the volumetric soil moisture content, electrical conductivity of the soil-water mixture, and contribution of surface charges to the bulk conductivity. Many techniques for measuring soil electrical conductivity have been proposed. However, all electrical conductance measurements, whether direct or indirect, suffer from similar difficulties, being that it is not water that conducts electricity, but rather the ions dissolved in the water (Zegelin, 1996).

2.1.4.1 *Electrical Conductivity Probes*

Electrical conductivity probes consist of both two and four electrode probe types. A four electrode probe is used to measure soil electrical conductivity in preference to a two electrode probe, as this eliminates the problem of contact resistance, by measuring current and voltage between different pairs of electrodes (Zegelin, 1996).

The principal advantages of the electrical conductivity probe for measuring soil moisture content are its ease of use, simplicity, low cost of equipment, and the relatively large volume of soil sampled (Zegelin, 1996).

2.1.4.2 *Electrical Resistance Blocks*

The direct insertion electrical conductivity probe technique of measuring electrical conductivity suffers, because of the differing contributions to bulk conductivity of surface charge and soil pore structure, and their spatial

distributions in field soils. To overcome these uncertainties, electrodes have been embedded in porous materials such as gypsum and fibreglass blocks (Zegelin, 1996).

This indirect technique relies on the equilibration of soil water potential in the block with that in the surrounding soil. Because of this, natural wetting and drying cycles give rise to hysteresis in the block response, so that blocks must be calibrated under both wetting and drying regimes (Zegelin, 1996).

The advantages of resistance blocks lie in their cheapness, their ease of installation, their relative simplicity of operation, and the fact that many blocks may be multiplexed from a single bridge (Zegelin, 1996). However, some resistance blocks have a high failure rate and are sensitive to soil rock content, resulting in over-estimation of soil moisture content and a need for in-situ calibration (Amer *et al.*, 1994).

2.1.4.3 Electromagnetic Induction

In the **Electromagnetic Induction (EMI)** technique, primary and secondary magnetic fields are imposed in the soil-water mixture through a transmitter coil placed on the soil surface. The ratio of these two fields at the receiver coil provide an estimate of the apparent electrical conductivity of the soil (Zegelin, 1996).

The major advantages of EMI are that it does not need to be inserted in the ground, it is easy and quick to operate, and can provide estimates over large areas and substantial depths (of order 10 m). A disadvantage of this method is that the task of isolating the effects from soil moisture content at a particular depth is difficult (Zegelin, 1996).

2.1.5 TENSIO METER METHOD

Tensiometers measure the capillary tension (energy with which water is held by the soil), through a liquid filled porous cup connected by a continuous liquid column to a manometer (Wilson, 1971; Schmugge *et al.*, 1980).

The advantages of this system are that they have relatively low cost, and can read both water table elevation and soil moisture tension. The disadvantages

are that they provide direct measurements of soil moisture tension but only indirect measurements of soil moisture content, can be easily broken during installation, and results can only be determined within the 0 to 800 cm water tension range (Schmugge *et al.*, 1980). In comparison, the permanent wilting point of plants is about 15000 cm (Wilson, 1971).

2.1.6 HYGROMETRIC METHOD

The relationship between moisture content in porous materials and the relative humidity of the immediate atmosphere is well known. Therefore, several relatively simple sensors for measuring relative humidity have been designed. Basically, these sensors can be classified into seven types of hygrometers: electrical resistance, capacitance, piezoelectric sorption, infra-red absorption and transmission, dimensionally varying element, dew point, and psychometric.

The advantages of the hygrometric method are simplicity of the apparatus and low cost. The disadvantages are deterioration of the sensing element through interactions with the soil components and the special calibration required for each material that is tested (Schmugge *et al.*, 1980).

2.1.7 SOIL DIELECTRIC METHOD

The dielectric constant (also known as permittivity or specific inductive capacity) ϵ , is a measure of how polarisable a material is when subjected to an electric field (Zegelin, 1996). This material property is usually measured relative to that of free space, and is referred to as the relative dielectric constant ϵ_r .

Soil consists of air, soil particles and water. Therefore the relative dielectric constant of soil is a composite of its components (Jackson *et al.*, 1996). Soil moisture content can be determined from measurements of the soil dielectric constant, as a result of the large difference between the relative dielectric properties of liquid water (approximately 80) and dry soil (2 to 5) (Jackson *et al.*, 1981; Schmugge, 1985; Engman and Chauhan, 1995). Since the dielectric constant is a volume property, the volumetric fraction of each component is involved. Thus, as the soil moisture content increases, the relative dielectric constant can increase to 20 or greater (Schmugge, 1985). Further details regarding

the dielectric behaviour of moist soil and the commonly used dielectric mixing models are given in a subsequent section.

2.1.7.1 Capacitance Probes

When a potential is placed across the plates of a capacitor containing a dielectric, charges induced by polarisation of the material act to counter the charges imposed on the plates. Hence, the capacitance between two parallel plates is a function of the dielectric constant of the dielectric (Zegelin, 1996).

Parallel plate probes have been widely used in laboratory determination of moisture content of porous materials, but their use in the field is less convenient because of the problem with plate insertion and soil disturbance. More recent capacitance probes are split cylindrical electrodes that may be buried in the soil or positioned at different depths down plastic access tubes embedded in soil (Zegelin, 1996).

The strengths of the modern probes include: (i) their ability to be left in-situ to log soil moisture content changes; (ii) the rapidity and ease of measurements; (iii) their extreme sensitivity to small changes in soil moisture content, particularly at dry soil moisture contents; (iv) their precise depth resolution; and (v) the relative cheapness of the probe. The weaknesses of the capacitance probe technique include: (i) the fact that there is a relatively small zone of influence for capacitance probes; (ii) their sensitivity to the region immediately adjacent to the probe; and (iii) their sensitivity to air gaps surrounding the probes (Zegelin, 1996).

2.1.7.2 Time Domain Reflectometry Probes

In **Time Domain Reflectometry (TDR)**, an electromagnetic wave is propagated along a wave guide embedded in a material whose dielectric constant is required. The down and return travel time t of the electromagnetic wave in the wave guide of length L , depends on the dielectric constant of the material in contact with the wave guide (D'Urso *et al.*, 1994; Zegelin, 1996). As the dielectric constant of the material in contact with the wave guide is increased, the speed of the electromagnetic wave decreases (Soil Moisture Equipment Corp., 1989;

Zegelin, 1996). In commercial TDR instruments, the reflections of multiple step electromagnetic waves due to impedance variations along the wave guide are sampled and recorded (D'Urso *et al.*, 1994). The analysis of such output allows for the measurement of travel time through the soil, and estimation of the propagation speed for the electromagnetic waves through the medium ($v = 2L/t$). In turn, assuming that the loss tangent is much less than 1, the average relative dielectric constant of the soil can then be derived from the velocity. This is achieved by using $v = c_0/\sqrt{\epsilon_r}$, where c_0 is the velocity of an electromagnetic wave in a vacuum ($\approx 3 \times 10^{10}$ cm s⁻¹) and ϵ_r is the relative dielectric constant (Soil Moisture Equipment Corp., 1989; D'Urso *et al.*, 1994; Zegelin, 1996).

Two wire probes (wave guides) are mismatched to the coaxial TDR system, and require a balancing transformer (balun) to be placed between the probes and the coaxial cable to reduce signal loss. However, the balun itself can be a source of noise and cause problems in analysing signals from short probes or probes in conducting soils. To overcome these problems, 3 and 4 wire probes have been used, which do not require a balun. The difficulty of insertion and degree of soil disturbance increases with the number of wires attached to the probe. The balance between this and signal clarity is reached by the 3 wire probe (Zegelin, 1996).

Vertically inserted TDR probes provide an average soil moisture content measurement over the depth of insertion, whilst probes inserted horizontally provide an average soil moisture content measurement at the plane of insertion. In addition, surface probes have been used to prevent soil disturbance and to measure soil moisture content close to the soil surface. However, these probes have about half the sensitivity to soil moisture content changes to that of insertion probes (Zegelin, 1996).

The advantages of TDR include: (i) the probes can be installed at any depth and accommodate automatic reading, allowing easy monitoring of the soil moisture profile; (ii) the portability of the technique; (iii) the approximately “universal” calibration curve for light textured soils, particularly at high soil moisture contents; and (iv) the precise depth resolution when horizontally inserted probes are used. The main disadvantages of the system include: (i) the relatively

small zone of influence of TDR probes and their sensitivity to the region immediately adjacent to the probe wires; (ii) the sensitivity to air gaps surrounding the probes; (iii) attenuation of the signal caused by salinity or highly conductive heavy clay soils; and (iv) the failure of the “universal” calibration curve for heavy clay soils and at low moisture contents (Schmugge *et al.*, 1980; Zegelin, 1996).

2.2 MICROWAVE DIELECTRIC BEHAVIOUR OF MOIST SOIL

Soil is a mixture of soil particles, air, and both bound and free water (Ulaby *et al.*, 1986). Microwave techniques for the measurement of soil moisture content rely on the clear distinction between the dielectric properties of water and those of the soil particles. The dielectric properties are measured by the dielectric constant ϵ , which is a complex number representing the response of a material to an applied electric field, such as an electromagnetic wave (Schmugge, 1985). This property consists of both real and imaginary parts by the relationship $\epsilon = \epsilon' + i\epsilon''$, and is usually measured relative to that of free space (ie. $\epsilon_r = \epsilon/\epsilon_0$).

The real (in phase) component of ϵ determines the propagation characteristics of the electromagnetic wave in the material (ie. its velocity), while the complex (out of phase) component determines the energy losses or absorption as the electromagnetic wave travels through the material (Schmugge, 1985; D’Urso *et al.*, 1994; Engman and Chauhan, 1995; Zegelin, 1996; Bolognani *et al.*, 1996), and is often referred to as the dielectric loss factor (Zegelin, 1996). The energy losses are due to vibration and/or rotation of the water molecules (Wütherich, 1997).

For dry soil particles, the real part of the relative dielectric constant ϵ_r' varies from a value of 2 to 5 (depending on soil bulk density) independent of frequency (Dobson and Ulaby, 1986a), with an imaginary part ϵ_r'' typically less than 0.05 (Ulaby *et al.*, 1996). In contrast, for free water the relative dielectric constant at 1 GHz and room temperature is approximately 80 for the real component and 4 for the imaginary component (Ulaby *et al.*, 1996). It is this large difference that makes the use of microwave techniques possible for the

measurement of soil moisture content, with the addition of water to soil causing the relative dielectric constant of the mixture to increase to a value of 20 or greater (Schmugge, 1985). However, like other mixtures involving water, the dielectric constant of the moist soil is not simply a weighted average of its components. The mixing model is complex and there are many influencing factors (Jackson and Schmugge, 1989).

The large value of ϵ_r for free water results from the fact that water is a polar molecule which is free to rotate along the direction of an applied electric field (Schmugge, 1985; Engman and Chauhan, 1995), allowing alignment of the water molecules electric dipoles (Engman, 1990). Bound water has a lower dielectric constant than free water contained in the pore spaces, because its water molecules are adsorbed to the surfaces of particles and the dipoles are immobilised (Jackson and Schmugge, 1989; Njoku and Entekhabi, 1996). Hence, dielectric mixing models need to account for the contributions to dielectric constant from both bound and free water. Furthermore, as the dielectric constant of moist soil is proportional to the number of water dipoles per unit volume, the preferred measurement for soil moisture content in the mixing models is volumetric, rather than gravimetric (Dobson and Ulaby, 1986a).

In addition to total moisture content, the degree of alignment of the water molecule dipoles (and thus the magnitude of ϵ) is a function of the observation frequency, soil temperature, soil texture and soil salinity (Topp *et al.*, 1980; Schmugge, 1985; Ulaby *et al.*, 1986; Heimovara, 1994). As soil temperature increases, ϵ' decreases because of the decreased dipole alignment resulting from thermal agitation. Roth *et al.* (1990) indicate that the most sensitive frequency range for soil moisture content determination from measurements of soil dielectric constant, lies between approximately 50 MHz and 10 GHz.

At frequencies below about 50 MHz, soil type has a marked impact on dielectric constant (Zegelin, 1996). However, in the normal microwave sensing range (0.4 to 10 GHz), the dielectric constant has relatively weak sensitivity to soil type. Figure 2.1 shows the relationship between dielectric constant and volumetric soil moisture content for a variety of soil types at a frequency of 1.4 GHz. The dependence on soil type is due to the different percentages of water

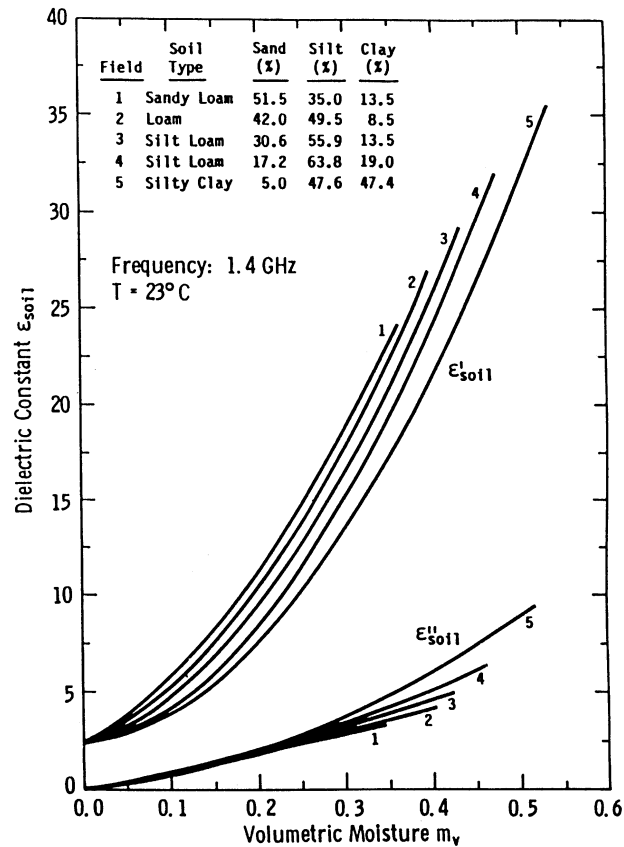


Figure 2.1: Dielectric constant as a function of volumetric soil moisture content for five soil types at 1.4 GHz and a soil temperature of 23°C. Smooth curves were drawn through measured data points (Ulaby *et al.*, 1986).

bound to the particle surfaces in the different soils (Dobson and Ulaby, 1986a; Njoku and Entekhabi, 1996) and the soil porosity (Dobson and Ulaby, 1986a). For soil moisture contents greater than 5% v/v, the soil porosity does not influence ϵ as long as the moisture content is expressed on a volumetric basis (Ulaby *et al.*, 1996).

The effect of salinity on the dielectric constant is to add an ionic conductivity term for ϵ'' . This produces a large increase in ϵ'' at low frequencies, but has little effect on ϵ' (Schmugge, 1985). Therefore, high soil salinity may significantly influence the soil dielectric properties. As the imaginary part of the dielectric constant is related to the electrical conductivity of the soil, it may be used to study soil salinity (Dalton and van Genuchten, 1986).

Several relationships between soil moisture content and the soil dielectric constant have been proposed. According to Topp *et al.* (1980), the volumetric soil

moisture content can be determined simply from the real part of the dielectric constant by means of an empirical regression equation. This regression equation was derived from multiple regression analysis of experimental data for frequencies between 1 MHz and 1 GHz. The main advantage of this relationship is that it does not require the determination of any soil parameters and does not require information on the observation frequency or soil temperature. Over this frequency range, Topp *et al.* (1980) found the real part of the dielectric constant to be almost independent of soil density, soil texture, soil salinity and soil temperature for temperatures between 10°C and 36°C. However, the validity of this relationship has not been demonstrated for the whole range of possible soil moisture contents and porosities (Roth *et al.*, 1990).

Wang and Schmugge (1980) have derived a simple empirical model to describe the observed dielectric constant of soil-water mixtures at frequencies between 1.4 and 5 GHz. In their model, the dielectric constant of a soil-water mixture is computed from the known dielectric constants of air, ice, dry soil and water, and the volume fraction of each constituent in the mixture. The frequency dependence of this model is imposed through the values given to the dielectric constant of water. Wang and Schmugge (1980) found that the relationship of dielectric constant to soil moisture content changed after reaching some transition moisture content, which varied with soil type. Hence, Wang and Schmugge (1980) presented two relationships for dielectric constant, depending on whether the soil moisture content is above or below the transition soil moisture content. An empirical relationship between the transition soil moisture content and the wilting point moisture content, given as a function of the sand and clay content, was also presented. The explanation given for this transition in dielectric constant with soil moisture content is as follows. The first water added to a soil is tightly bound to the surface of the soil particles, thus inhibiting the rotational motion of the dipole. As more water is added, the water molecules are further away from the surface of the particles and may rotate more freely. Since the surface area in a soil depends on its particle size distribution, clay soils can hold more of this tightly bound water than sandy soils (Schmugge, 1985).

Hallikainen *et al.* (1985) have derived empirical relationships with separate polynomial expressions for both the real and imaginary parts of the

dielectric constant between observation frequencies of 1.4 and 18 GHz. These polynomial expressions relate the real and imaginary parts of the complex dielectric constant, to the volumetric soil moisture content and the percentages of sand and clay, with coefficients that depend on the observation frequency.

Dobson *et al.* (1985) have presented both theoretical and semi-empirical dielectric mixing models. The theoretical model apportions the soil-water mixture into a bound water volume fraction and a free water volume fraction, in accordance with the pore-size distribution calculated from the particle size distribution. The mixing model uses a multi-phase formula for a mixture containing randomly oriented inclusions. The mixture consists of the soil solid as host material and three types of inclusions (bound water, free water, and air), all of which are assumed to be disc-shaped and whose size is governed by the particle-size distribution and total amount of water in the mixture.

The semi-empirical dielectric mixing model of Dobson *et al.* (1985) gives the dielectric constant as a function of soil temperature, soil moisture content, soil texture, and observation frequency, for both the real and imaginary parts of the dielectric constant. This model is valid for frequencies between 1.4 and 18 GHz. Dobson *et al.* (1985) showed their semi-empirical mixing model to yield an excellent fit to the measured data at frequencies above 4 GHz. At frequencies less than this, the mixing model does not fully account for the dielectric properties of bound water at low soil moisture contents. It has also been noted that if the model is limited to frequencies higher than 4 GHz, the effects of soil salinity may be ignored (Ulaby *et al.*, 1986).

Peplinski *et al.* (1995) have extended the semi-empirical dielectric mixing model of Dobson *et al.* (1985) to be valid over the whole range of frequencies between 0.3 and 18 GHz. In this mixing model, a small linear adjustment has been introduced to correct the expression of Dobson *et al.* (1985) for the real part of the relative dielectric constant, at frequencies between 0.3 and 1.3 GHz. For the imaginary part of the relative dielectric constant, a new equation was proposed for the effective conductivity σ_{eff} at frequencies between 0.3 and 1.3 GHz.

The model of Peplinski *et al.* (1995) is currently the most commonly used soil-water-air dielectric mixing model, being a compromise between the

complexity of the theoretical model and the simplicity of the empirical models. Furthermore, this mixing model has the widest validity range in terms of observation frequency and accounts for the most important factors, including observation frequency, soil texture and soil temperature. This model is presented below in terms of the volumetric soil moisture fraction θ , soil bulk density ρ_b (g cm^{-3}), soil specific density ρ_s ($\approx 2.66 \text{ g cm}^{-3}$), and an empirically determined constant $\nu = 0.65$.

$$\varepsilon'_r = \left[1 + \frac{\rho_b}{\rho_s} (\varepsilon_s^\nu - 1) + \theta^{\beta'} \varepsilon'_{fw}{}^\nu - \theta \right]^{\frac{1}{\nu}} \quad (2.2a)$$

$$\varepsilon''_r = \left[\theta^{\beta''} \varepsilon''_{fw}{}^\nu \right]^{\frac{1}{\nu}} \quad (2.2b),$$

where β' and β'' are empirically determined soil type constants expressed as a function of the sand (S) and clay (C) mass fractions by

$$\beta' = 1.2748 - 0.519S - 0.152C \quad (2.3a)$$

$$\beta'' = 1.33797 - 0.603S - 0.166C \quad (2.3b).$$

The quantities ε'_{fw} and ε''_{fw} are the real and imaginary parts of the relative dielectric constant of free water respectively, given by

$$\varepsilon'_{fw} = \varepsilon_{w\infty} + \frac{\varepsilon_{w0} - \varepsilon_{w\infty}}{1 + (2\pi f\tau_w)^2} \quad (2.4a)$$

$$\varepsilon''_{fw} = \frac{2\pi f\tau_w (\varepsilon_{w0} - \varepsilon_{w\infty})}{1 + (2\pi f\tau_w)^2} + \frac{\sigma_{eff}}{2\pi\varepsilon_o f} \frac{(\rho_s - \rho_b)}{\rho_s \theta} \quad (2.4b),$$

where $\varepsilon_{w\infty} = 4.9$ is the high frequency limit of ε'_{fw} , ε_o is the dielectric constant of free space ($8.854 \times 10^{-12} \text{ F.m}^{-1}$), and f is the observation frequency in Hertz.

The relative dielectric constant of the soil solids ϵ_s , is given by the relationship

$$\epsilon_s = (1.01 + 0.44\rho_s)^2 - 0.062 \quad (2.5).$$

For frequencies between 0.3 and 1.3 GHz the real part of the relative dielectric constant is given by the linear adjustment in (2.6), while for frequencies between 1.4 and 18 GHz it is given directly by (2.2a).

$$\epsilon'_r = 1.15\epsilon'_{r(2.2a)} - 0.68 \quad (2.6),$$

where $\epsilon'_{r(2.2a)}$ is the real component of the relative dielectric constant from (2.2a).

In evaluating the imaginary part of the relative dielectric constant, the effective conductivity given in (2.7a) is used for frequencies between 0.3 and 1.3 GHz, while that given in (2.7b) is used for frequencies between 1.4 and 18 GHz.

$$\sigma_{eff} = 0.0467 + 0.22049\rho_b - 0.4111S + 0.6614C \quad (2.7a)$$

$$\sigma_{eff} = -1.645 + 1.939\rho_b - 2.25622S + 1.594C \quad (2.7b)$$

The relaxation time for water τ_w and the static dielectric constant of water ϵ_{wo} are given as a function of soil temperature T (°C) by (Ulaby *et al.*, 1986)

$$2\pi\tau_w(T) = 1.1109 \times 10^{-10} - 3.824 \times 10^{-12}T + 6.938 \times 10^{-14}T^2 - 5.096 \times 10^{-16}T^3 \quad (2.8)$$

$$\epsilon_{wo}(T) = 88.045 - 0.4147T + 6.2958 \times 10^{-4}T^2 + 1.075 \times 10^{-5}T^3 \quad (2.9).$$

The necessity of using (2.7a) to evaluate the imaginary part of the relative dielectric constant for frequencies less than 1.3 GHz and (2.7b) for frequencies

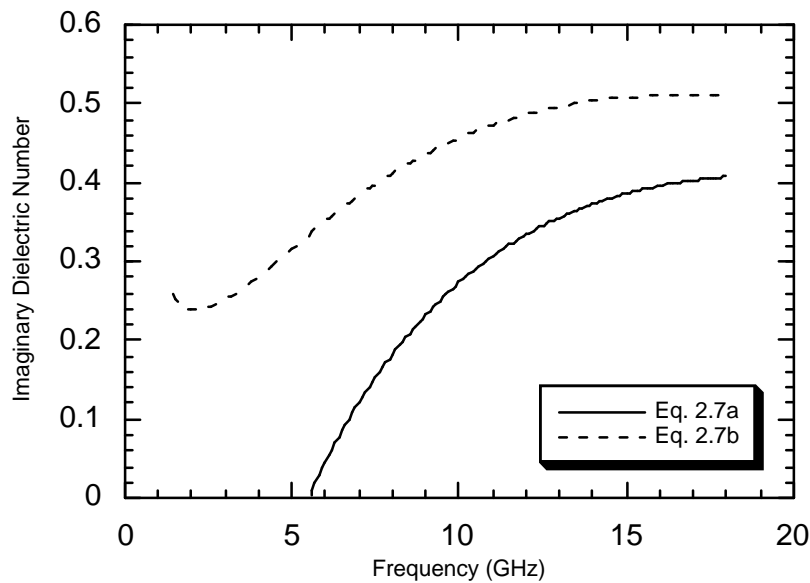


Figure 2.2: Plot of the imaginary part of the relative dielectric constant for a volumetric soil moisture content of 5% v/v, using the effective conductivity given by (2.7a) and (2.7b).

greater than 1.4 GHz has been investigated as part of this thesis. By evaluating ϵ_r'' using both relationships for two soil moisture conditions over the frequency range of 1.4 to 18 GHz, the sensitivity of estimating the imaginary relative dielectric constant at frequencies less than 1.3 GHz with (2.7b) is illustrated. The results of this analysis are given in Figure 2.2 for 5% volumetric soil moisture content and Figure 2.3 for 40% volumetric soil moisture content.

From Figure 2.2 and Figure 2.3, it can be seen that the difference introduced in evaluation of ϵ_r'' by using (2.7a) for frequencies greater than 1.4 GHz is greatest for low frequencies and high soil moisture content, with a maximum variation in ϵ_r'' of 2. It would therefore appear that the relationship for effective conductivity given in (2.7a) may be used over the range of frequencies from 0.3 to 18 GHz, given the variation in the data used to derive the relationship.

The above dielectric constant model of Peplinski *et al.* (1995) was also evaluated for two soil moisture conditions and four soil temperature states, with the results given in Figure 2.4 and Figure 2.5. The purpose of this investigation was to quantify the contribution of the imaginary part of the relative dielectric constant to the complex dielectric constant, and the sensitivity of the dielectric model to observation frequency and soil temperature as a function of soil moisture content.

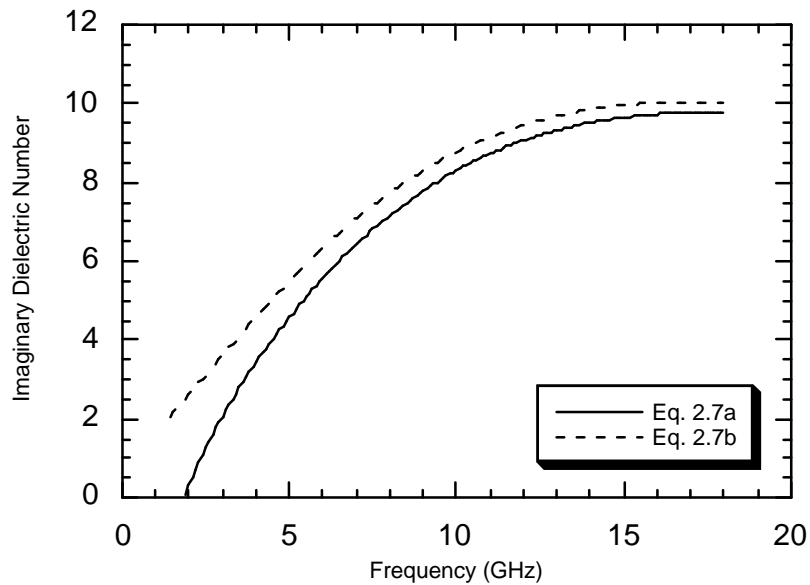


Figure 2.3: Plot of the imaginary part of the relative dielectric constant for a volumetric soil moisture content of 40% v/v, using the effective conductivity given by (2.7a) and (2.7b).

The results of this analysis indicate that frequency dependence is greatest at low soil temperatures and high soil moisture content, and temperature dependence is significantly greater at high soil moisture contents and high frequencies. This observation has been noted already by Hoekstra and Delaney (1974) and Roth *et al.* (1990). Decreasing the soil temperature below 0°C produces a substantial reduction in both the real and imaginary parts of the dielectric constant due to the freezing of water (Hallikainen *et al.*, 1985).

Figure 2.4 and Figure 2.5 also indicate that the temperature effect on the real part of the relative dielectric constant is minimised at frequencies of 4 to 6 GHz (C-Band). However, this coincides approximately with the maximum variation in the imaginary part of the relative dielectric constant. The results further indicate that at high soil moisture content and low soil temperature, the real and imaginary parts of the relative dielectric constant may be approximately equal for high frequencies. However, at low moisture content the imaginary component may be as low as approximately one-tenth of the real component, irrespective of soil temperature and observation frequency.

As it is possible for variations in near-surface soil temperature of up to 50°C during any single day in some parts of the world, the results of this investigation would indicate that soil temperature cannot be ignored in evaluating

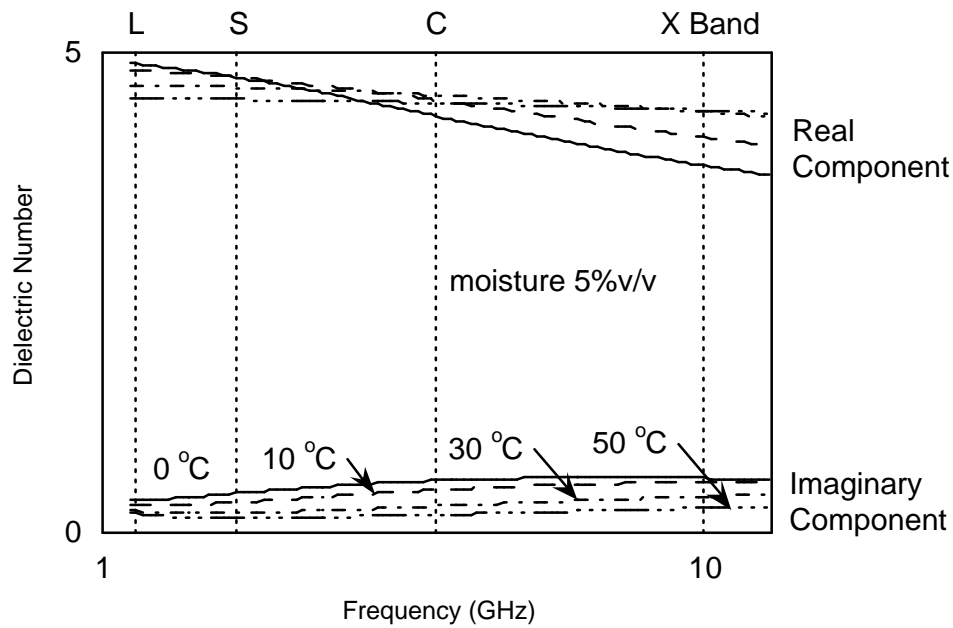


Figure 2.4: Plot of real and imaginary components of the complex relative dielectric constant for a soil at 5% volumetric moisture content, with soil temperatures of 0, 10, 30 and 50°C.

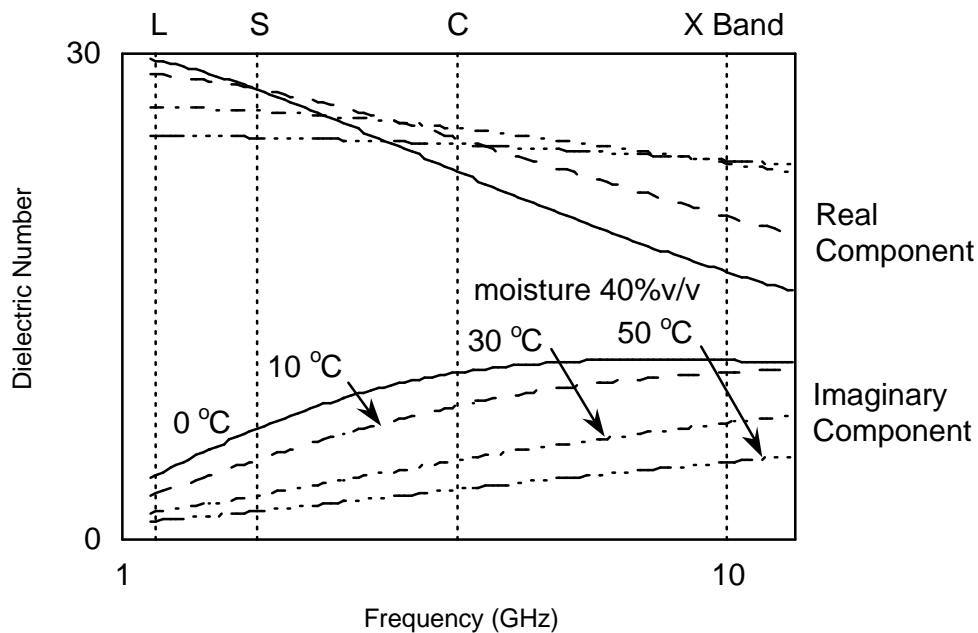


Figure 2.5: Plot of real and imaginary components of the complex relative dielectric constant for a soil at 40% volumetric moisture content, with soil temperatures of 0, 10, 30 and 50°C.

the soil dielectric constant. It would also appear that observation frequency needs to be accounted for in evaluating the dielectric constant, and the imaginary component of the dielectric constant should not be disregarded, as suggested by some researchers (eg. Chen *et al.*, 1995; Jackson *et al.*, 1996) especially for high observation frequency and soil moisture content.

2.3 REMOTE SENSING SYSTEMS

This section gives a short review of the remote sensing systems that are currently available. Firstly, there is a short discussion of the types of platforms that have been used for carrying the remote sensing instruments, including the advantages and disadvantages of each. This is followed by a review of the main types of remote sensing instruments that are used by the various remote sensing systems, and finally there is a brief review of the most commonly used remote sensing satellites.

2.3.1 REMOTE SENSING PLATFORMS

Platforms for supporting remote sensing instruments have varied from ground-based supports to aircraft and satellites. Ground-based systems can be mounted on trucks or on special structures such as rails, which allow limited movement of the sensor. The main application of these types of platforms is in the development of new sensor systems and the verification of sensor response with respect to target characteristics. An example of a truck-mounted sensor is given in Figure 2.6. The advantage of these systems is the relatively small footprint of the sensor, allowing for easier control of the conditions under which the measurements are made (Jackson *et al.*, 1996). However, a major disadvantage of the ground-based systems is their limitations on coverage of large areas (Bolognani and Altese, 1994).

This situation is partly overcome by the adoption of aircraft mounted systems. Aircraft based instruments are especially useful in the mapping of large areas, and can also serve as prototypes for future satellite sensors. In most cases they offer better spatial resolution than satellite systems as well as more control over the frequency and timing of coverage (Jackson *et al.*, 1996).



Figure 2.6: An example of a ground-based system. The system comprises a "truck"-mounted radiometer, making observations of a sand target area. Data processing equipment is contained within the van (Njoku and Kong, 1977).

Satellite based remote sensing provides the optimal solution, due to the capability of monitoring large areas with long term repetitive coverage. However, the length of the repeat cycle (time between satellite overpasses of the same area on the ground) can be a critical problem in studies involving rapidly changing conditions, such as soil moisture (Jackson *et al.*, 1996).

2.3.2 SENSOR TYPES

The most commonly used remote sensing instruments in the field of soil moisture estimation are the **Multi-Spectral Scanner (MSS)**, **Thematic Mapper (TM)**, thermal infra-red line scanner, microwave radiometer and the **Synthetic Aperture Radar (SAR)**.

2.3.2.1 *Multi-Spectral Scanner*

The MSS has a very high radiometric resolution in narrow and simultaneously recorded wavebands, covering wavelengths in the electromagnetic spectrum from ultra-violet ($0.3 \mu\text{m}$) to thermal infra-red wavelengths ($14 \mu\text{m}$) (Curran, 1985). MSSs measure the radiance of the earth's surface along a scan line, perpendicular to the line of flight, by use of either a rotating mirror (whisk-broom) or a linear array of detectors (push-broom). The advantage of push-broom scanners over whisk-broom is that they allow a longer dwell time over which to

measure the energy from each ground resolution cell. This enables a much stronger signal to be recorded and a greater range in the levels of signal that can be sensed. The disadvantages of the push-broom arrangement are that many more detectors require calibration, and they are not readily available for wavelengths longer than near infra-red (Lillesand and Kiefer, 1994).

2.3.2.2 Thematic Mapper

The TM is a highly advanced sensor incorporating a number of spectral, radiometric and geometric design improvements relative to the MSS, covering wavelengths from blue (0.45 μm) to thermal infra-red (12.5 μm). Unlike the MSS, the TM uses a bi-directional whisk-broom scanner that employs an increased number of sensors in comparison to the MSS, allowing for an increase in resolution. The TM has the added advantage over the MSS in that it measures spectral radiance over a range of 256 digital numbers rather than 64 (Lillesand and Kiefer, 1994).

2.3.2.3 Thermal Infra-Red Linescanner

Thermal infra-red line scanners are a particular type of whisk-broom MSS whose detector only senses in the thermal portion of the spectrum. These sensors usually collect data in two different wavebands, defined by the two atmospheric windows with least atmospheric attenuation, located between the wavelengths of 3 and 5 μm and between 8 and 14 μm (Lillesand and Kiefer, 1994). Thermal infra-red line scanners are now commonly part of the MSS mentioned above (Curran, 1985).

2.3.2.4 Microwave Radiometer

Passive microwave remote sensors are radiometers that measure the thermal emission from the ground at microwave wavelengths. These radiometers are similar to thermal scanners, but have antennas rather than photon detectors, and scan a scene by having a multiple antenna array. As radiometers measure a very weak signal, measurement of the thermal emission requires very sensitive instruments. These sensors consist of a large antenna, and a very sensitive radio receiver, in order to collect enough energy to yield a detectable signal. The effect

of having a large antenna is to have a large beam width, and hence poor spatial resolution (Lillesand and Kiefer, 1994). Calibration of microwave radiometers is generally made in-flight over large bodies of water (Wang *et al.*, 1987).

2.3.2.5 Synthetic Aperture Radar

Active microwave remote sensors are known as radars, from the acronym for **RA**dio **D**etection **A**nd **R**anging. A typical radar sensor consists of a transmitter and an antenna. The transmitter produces pulses of electromagnetic energy at microwave wavelengths, which are timed by a synchroniser and standardised to a known power by a modulator. For a fraction of a second the transmit/receive switch is switched to transmit, as the transmitter releases a microwave pulse from the antenna. The transmit/receive switch then returns to its original position and the antenna receives echoes corresponding to backscattering by objects located on the transmitted wave path (Curran, 1985; Barbier, 1996). The information that can be extracted from these echoes is two-fold. Firstly, the *distance* from the target to the radar can be determined by measuring the time delay between pulse transmission and reception of the corresponding echo. Secondly, the relative intensity of the echo provides a measure of the target reflectivity and is known as the *backscattering coefficient* σ^0 (Barbier, 1996). The backscattering coefficient, usually in decibels (dB), is evaluated from the ratio of the backscattered power to the emitted power (Fung, 1994).

The spatial resolution of radar data is controlled by the pulse length and the antenna beam width, which is governed by the length of the antenna. Thus, by increasing the length of the antenna, radar data with a finer resolution may be obtained. Due to the physical constraints in having an antenna of sufficient length to produce the desired resolution (10 m resolution requires a 4 km long antenna), the antenna length is simulated by appropriate processing of a large number of return signals along the flight trajectory. This process of synthesising a long antenna is known as SAR (Barbier, 1996).

Electromagnetic waves may be either horizontally (*h*) or vertically (*v*) polarised, with *h* polarised waves having an electric field parallel to the soil surface and *v* polarised waves having an electric field perpendicular to the soil

surface (Schmugge *et al.*, 1980). If an incident electromagnetic wave is h polarised, the energy backscattered towards the radar will, in general, consist of an electromagnetic wave that is also h polarised, as well as an electromagnetic wave that is v polarised. The latter is referred to as cross-polarised. Radars are capable of measuring the backscattering response for various polarisation configurations. A polarimetric radar is capable of measuring the radar response for vv , hh , hv , and vh , where the first letter denotes the polarisation of the transmit antenna and the second letter denotes the polarisation of the receive antenna. Because of the reciprocity property of radar scattering, the responses for hv and vh are identical (Ulaby *et al.*, 1996).

SAR can provide a unique perspective on the spatial and temporal variation in soil moisture content both at a relatively high resolution and at a global scale, because of its' characteristically high resolution combined with a global coverage. Furthermore, the increased number of SAR systems has made SAR data more readily available (Dubois and van Zyl, 1994).

2.3.3 REMOTE SENSING SATELLITES

Although numerous remote sensing systems are in existence and have been used for measurement of soil moisture content, only the most appropriate satellite systems for soil moisture measurement are discussed below.

In the case of passive microwave systems, there are no appropriate satellite systems currently available for soil moisture measurement. Hence, all large area research has utilised aircraft sensors. In recent years NASA has supported two airborne L-Band radiometers, the **Push-Broom Microwave Radiometer (PBMR)** and the **Electronically Scanned Thinned Array Radiometer (ESTAR)**. The ESTAR instrument doubles the number of footprints to eight, which makes it a more efficient mapping instrument. It is also a prototype for a new synthetic aperture antenna technology that can potentially solve the high altitude spatial resolution problem. There are three planned multiple wavelength satellite systems that will include C-Band microwave radiometers: the **Multi-frequency Imaging Microwave Radiometer (MIMR)**, the **Advanced Microwave Scanning Radiometer (AMSR)**, and the Russian system **PRIRODA** (Jackson *et al.*, 1996).

2.3.3.1 Landsat

The United States Landsat 5 (Figure 2.7) was launched in 1984 with a MSS and TM in a near-polar sun-synchronous orbit of 705 km altitude having a repeat cycle of 16 days. The MSS has 4 bands, being green, red, near infra-red and infra-red, with a swath of 185 km and pixel size of 82 m. The TM has 7 bands, being blue, green, red, near infra-red, near mid infra-red, mid infra-red and thermal infra-red. The TM has a swath of 185 km and pixel size of 30 m, except for the thermal infra-red band which is 120 m (Lillesand and Kiefer, 1994).

2.3.3.2 Systeme Pour l'Observation de la Terre

The SPOT (Systeme Pour l'Observation de la Terre) satellites are a French system developed in conjunction with Sweden and Belgium. SPOT 3 (Figure 2.8) is the current satellite, and was launched in 1993 into a sun-synchronous orbit with an altitude of 832 km and repeat cycle of 26 days. However, due to the possibility of varying the satellite look angle of pointing by $\pm 27^\circ$ using a mirror, it is possible to have up to 11 repeat images in a 26 day period. SPOT 3 has two push-broom **H**igh **R**esolution **V**isible (HRV) sensors that can operate in both multi-spectral and panchromatic (black and white) modes, with a swath of 60 km. When operating in the multi-spectral mode it can obtain data in three bands, being green, red, and infra-red, with a pixel size of 20 m. In the panchromatic mode, it has a resolution of 10 m. SPOT images also measure spectral radiance over a range of 256 digital numbers (Lillesand and Kiefer, 1994).

2.3.3.3 European Remote Sensing Satellite

The **E**uropean **R**emote **S**ensing (ERS-2) satellite was launched in 1995 and carries on board various advanced instruments for earth observation (Figure 2.9). Of interest for hydrologic applications is the **A**ctive **M**icrowave **I**nstrument (AMI), which comprises two separate radars: a SAR and a wind scatterometer. The AMI-SAR instrument operates at C-Band (5.3 GHz) with a *vv* polarisation. In SAR image mode it provides high resolution two-dimensional images with a spatial resolution of 26 m in range and between 6 and 30 m in

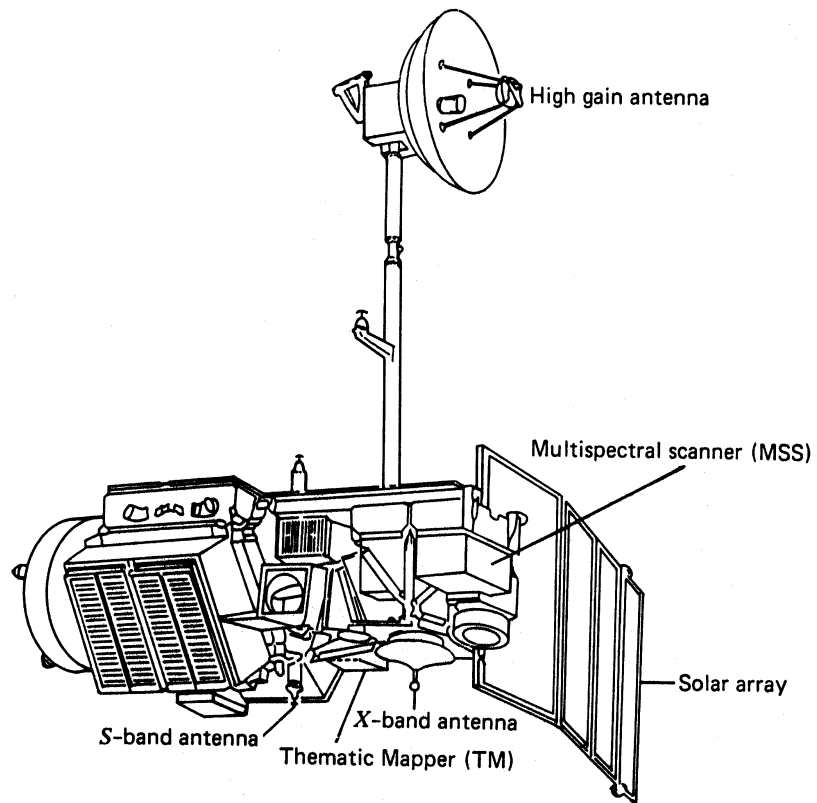


Figure 2.7: Landsat 5 satellite configuration (Lillesand and Kiefer, 1994).

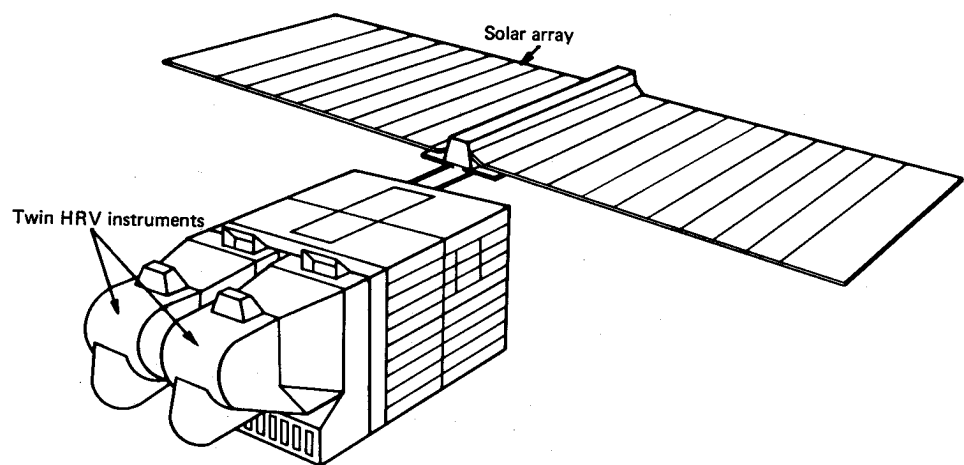


Figure 2.8: SPOT 3 satellite configuration (Lillesand and Kiefer, 1994).

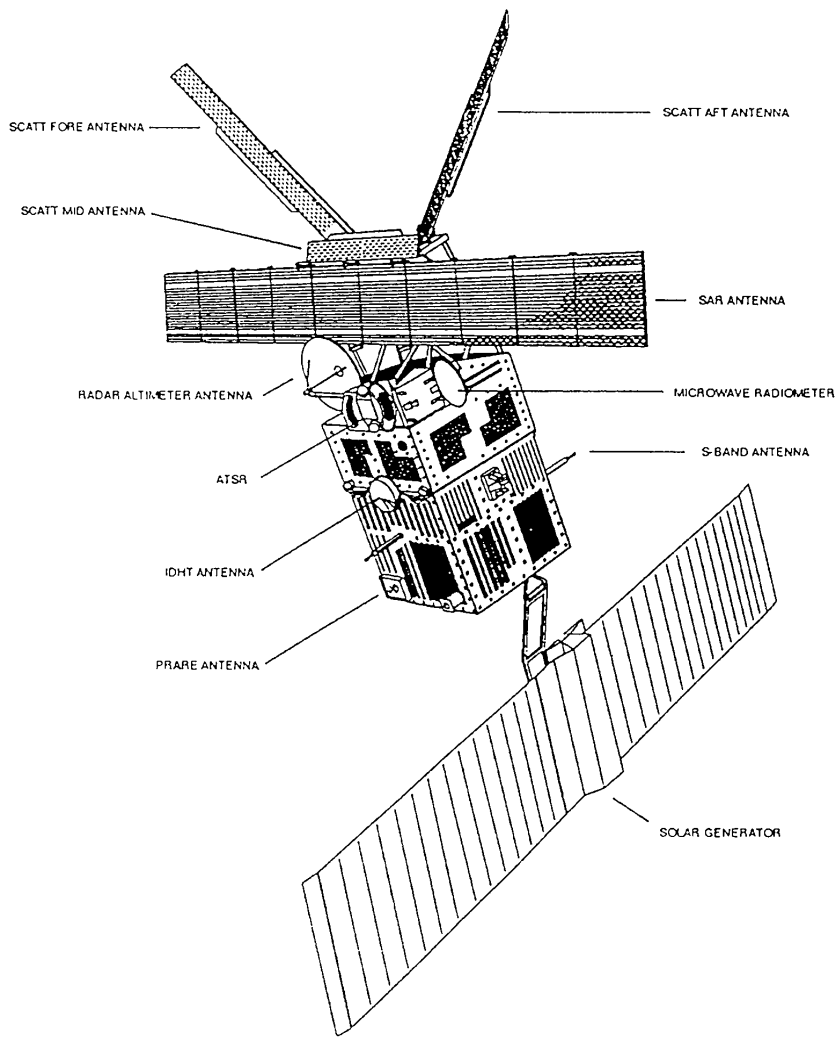


Figure 2.9: ERS-2 satellite configuration (Bolognani and Altese, 1994).

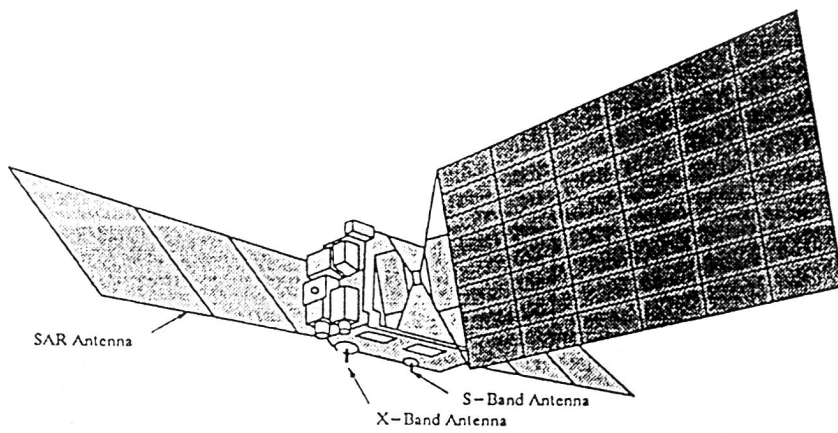


Figure 2.10: JERS-1 satellite configuration (Bolognani and Altese, 1994).

azimuth. ERS precision radar images are 3 look images corrected for the in-flight SAR antenna pattern and compensated for range spreading loss with a pixel size of 12.5 m × 12.5 m (D'Urso *et al.*, 1994). The satellite has a swath of 100 km to the right side of the satellite track. The mid swath incidence angle of the system in normal operation mode is 23°. The ERS satellite has a sun-synchronous orbit of 785 km with a repeat cycle of 35 days repeat cycle, and also has an infra-red radiometer on board (Bolognani and Altese, 1994; Lillesand and Kiefer, 1994; Su *et al.*, 1995).

2.3.3.4 Japanese Earth Resources Satellite

The Japanese Earth Resources Satellite (JERS-1) was launched in February 1992 and carries on board a 1.2 GHz (L-Band) SAR instrument with *hh* polarisation (Figure 2.10). The spatial and temporal resolutions of this sun-synchronous polar orbiting satellite at 568 km altitude are comparable with the ERS-2 satellite, having a swath width of 75 km, pixel size of 18 m and repeat cycle of 44 days. The mid swath incidence angle of this system in normal operation is 35°. JERS-1 also has an optical sensor that operates in 5 bands, consisting of 2 visible and 3 near infra-red bands (Lillesand and Kiefer, 1994).

2.3.3.5 RADARSAT

The Canadian RADAR SATellite (RADARSAT) was launched in 1995 with a C-Band *hh* polarisation SAR instrument (Figure 2.11). The RADARSAT SAR has the unique ability to shape and steer its radar beam to image swaths from 35 km to 500 km, with resolutions from 10 m to 100 m respectively. Incidence angles can also be varied from less than 20° to more than 50°. RADARSAT is in a sun-synchronous polar orbit at an altitude of 798 km, with a repeat cycle every 6 days using the 500 km swath and every 24 days using the standard 100 km swath mode (Lillesand and Kiefer, 1994; <http://radarsat.space.gc.ca/eng/radarsat/description.html>). RADARSAT also has the ability to swing the SAR beam from the right to the left side (Ahmed *et al.*, 1990).

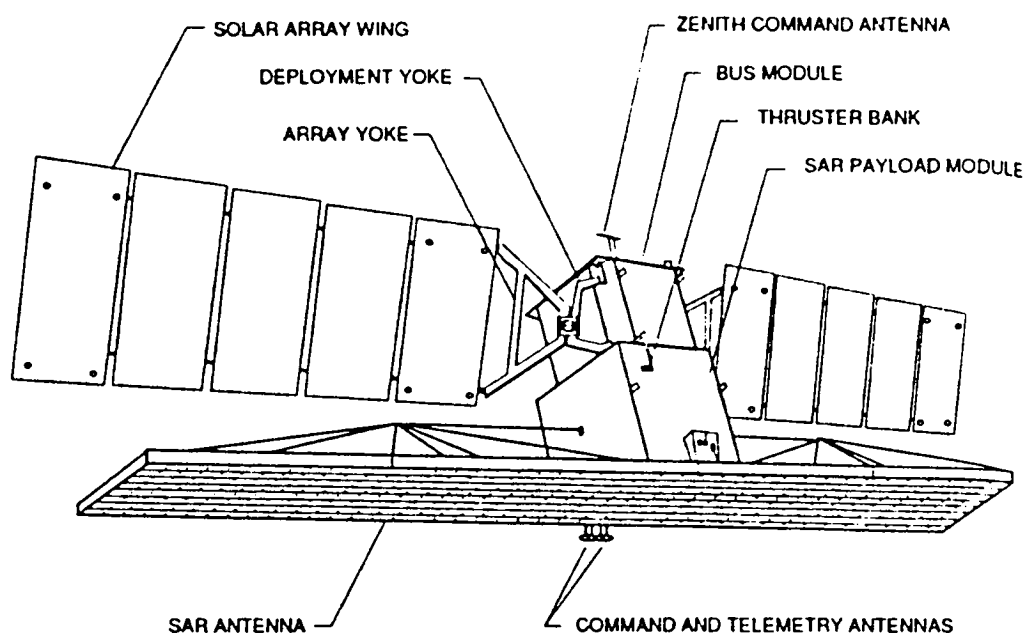


Figure 2.11: RADARSAT satellite configuration (Ahmed *et al.*, 1990).

2.4 REMOTE SENSING MEASUREMENT OF NEAR-SURFACE SOIL MOISTURE

While remote sensing can be defined as any non-contact method of determining information regarding an object's nature, properties or state, in this thesis it will be defined as the acquisition of digital data, either reflected or emitted by the earth's surface, in the visible, thermal or microwave portions of the electromagnetic spectrum (McVicar and Jupp, 1998).

Numerous researchers have shown that near-surface soil moisture content can be measured by visible and thermal infra-red remote sensing, as well as active and passive microwave remote sensing techniques. The main difference between these four techniques is the wavelength region of the electromagnetic spectrum that is used by the sensor, and the source of the electromagnetic energy. This section presents an overview of the current state of near-surface soil moisture measurement from these four types of remote sensing observations. A summary of the relative merits of the different remote sensing techniques is provided in Table 2.1.

Table 2.1: Summary of remote sensing techniques for measurement of near-surface soil moisture content (Schmugge *et al.*, 1979 and Engman, 1991).

	Property Observed	Advantages	Limitations	Noise Sources
Visible	Soil Albedo Index of refraction	Lots of data	Many noise sources	Numerous
Thermal Infra-Red	Surface temperature	High resolution Large swath Coverage frequency Physics well understood	Cloud cover limits frequency of coverage	Meteorological conditions Topography Vegetation cover
Active Microwave	Backscatter coefficient Dielectric properties	Low atmospheric noise High resolution	Limited swath width Calibration of SAR	Roughness Surface slope Vegetation cover
Passive Microwave	Brightness temperature Dielectric properties Soil temperature	Low atmospheric noise Moderate vegetation penetration	Low Resolution Man made radiation limits operating range	Roughness Vegetation cover Temperature

As remote sensors do not measure soil moisture content directly, mathematical models that relate the measured response of a particular remote sensing system to the soil moisture content must be derived (de Troch *et al.*, 1996). Forward modelling develops a set of mathematical relationships to simulate the instrument's response for a given set of model parameters. In the context of soil moisture remote sensing, these parameters generally include soil properties and the geometry and phenology of the overlying vegetation canopy. To solve the inverse problem, it is crucial to choose a forward modelling procedure that adequately describes the observations. It is also important to know how many model parameters should be used to depict the subjects being measured, and which parameters are most sensitive to the returned signal (Su *et al.*, 1995).

An alternative approach to that of finding an exact relationship between remote sensing observations and near-surface soil moisture content for active microwave observations is through change detection (Engman, 1990; Kite and Pietroniro, 1996). The change detection method minimises the impact of target variables such as soil texture, surface roughness, and vegetation, because these tend to change slowly, if at all, with time (Engman and Chauhan, 1995). Thus, it is assumed that the only change in the target is from a change in soil moisture content (Engman, 1990). This approach for measuring the near-surface soil moisture content is not reviewed in this thesis.

Due to the limitations of measuring near-surface soil moisture content with remote sensing in the visible region of the electromagnetic spectrum, only a very brief overview is given. Discussion is concentrated on near-surface soil moisture measurement from passive and active microwave remote sensing, with detailed explanation of the interpretation algorithms currently proposed.

2.4.1 VISIBLE REMOTE SENSING

Remote sensing of near-surface soil moisture content using the visible region of the electromagnetic spectrum measures the reflected radiation of the sun from the earth's surface, known as albedo (Sadeghi *et al.*, 1984), and uses wavelengths between 0.4 and 0.8 μm . Soil albedo is defined as the ratio of reflected to incoming radiation (Idso *et al.*, 1975), and has long been recognised as having a dependence upon the moisture status of the soil surface (Ångström, 1925). The effect of increasing soil moisture content is to reduce the albedo by a factor of about 2 for all soils except sands (Jackson *et al.*, 1976). However, this provides only a poor indication of soil moisture content, since soil reflectance is also influenced by organic matter, soil texture, surface roughness, angle of incidence, plant cover and colour (Engman, 1991; de Troch *et al.*, 1996), causing a wide variation in albedo of different soil types even when dry (Sadeghi *et al.*, 1984). These complicating factors, plus the fact that reflected solar energy responds to only the top few millimetres of the soil profile (Idso *et al.*, 1975), limit the utility of solar reflectance measurements for soil moisture content determination, and thus will not be further discussed in this thesis.

2.4.2 THERMAL INFRA-RED REMOTE SENSING

Thermal infra-red remote sensing operates in a slightly longer wavelength region of the electromagnetic spectrum (3 to 14 μm) than visible remote sensing, and measures the thermal emission of the earth (Curran, 1985).

Methods for inferring near-surface soil moisture content using thermal infra-red remote sensors rely upon using the thermal infra-red data to measure the soil surface temperature, as soil moisture influences the thermal properties of the soil. The difficulty with this is that radiation emitted from the soil surface and

measured by the remote sensor depends both on surface temperature and emissivity, after correction for atmospheric effects. Therefore, measurement of the soil surface temperature requires either measuring, or making an assumption about, the soil surface emissivity (Ottlé and Vidal-Madjar, 1994).

As soil moisture content has a strong influence on the thermal properties (heat capacity, thermal conductivity and latent heat of vaporisation of water) of the earth's surface, relatively minor changes in moisture content have a large effect on the bulk thermal properties of the ground (Ellyett and Pratt, 1975). Thus, areas having higher soil moisture content are cooler during the day and warmer at night (van de Griend and Engman, 1985).

The amplitude of the diurnal range of soil surface temperature is a function of both internal and external factors. The internal factors are the soil thermal conductivity λ and the soil heat capacity C_p , where $P = \sqrt{(\lambda C_p)}$ defines what is known as the soil thermal inertia. The external factors are primarily meteorological: solar radiation, air temperature, relative humidity, cloudiness and wind. The combined effect of these external factors is what drives the diurnal variation of soil surface temperature, while the thermal inertia is an indication of the soil's resistance to these driving forces (Schmugge *et al.*, 1980). To accentuate the difference in thermal properties of moist and dry areas, data is ideally collected around midday (Pickerill and Malthus, 1998).

In addition to one time of day thermal infra-red observations for inferring soil moisture content, day-night temperature differences may be used. The difference between day and night surface temperature is a function of the thermal inertia of the system, which is controlled by the amount of water in the soil. For a given soil in a wet phase, the diurnal temperature range will be smaller than for dry soils, with everything else being equal (McVicar and Jupp, 1998). The amplitude of the diurnal range of soil surface temperature has been found to have a good correlation with the soil moisture content in the 0 to 2 and 0 to 4 cm layers of the soil (Schmugge *et al.*, 1980).

The effectiveness of thermal infra-red measurements is limited by cloud cover, vegetation and meteorological factors (Engman, 1990; de Troch *et al.*, 1996), with measurements being severely hampered by the presence of even slight

amounts of vegetation (Sadeghi *et al.*, 1984). If the vegetation cover consists of brush or trees, and obscures more than about 10 to 20% of the soil surface, then the resulting image produced by the remote sensor may have no relation to the radiation temperature of the earth's surface below. If the vegetation cover is predominantly low grass, then the resulting image is closely related to the earth's surface temperature (Ellyett and Pratt, 1975).

For densely vegetated soils, the plant canopy temperature difference with the surrounding air yields information about the soil moisture status (van de Griend and Engman, 1985). However, the use of thermally emitted radiation over dense vegetation to deduce substrate moisture is complex, due to the soil-vegetation-atmosphere interaction. Furthermore, leaf temperature does not rise very far above air temperature until very low soil moisture contents are reached, because the plant makes use of the available water in the root zone (Wüthrich, 1997). However, thermal infra-red observations may be used to give an indication of plant moisture stress through rising leaf temperatures (McVicar and Jupp, 1998). Because of the complicating factors from vegetation, inference of soil moisture content from thermal infra-red imagery is usually performed in conjunction with imagery from the visible wave bands, in order to give some measure of the vegetation cover. Several of the approaches that have been used to infer near-surface soil moisture content from thermal infra-red remote sensing are described below.

Jordon and Shih (1993) have investigated the possibility of inferring soil moisture content using thermal infra-red observations alone. In their approach, they considered bare soil covered with a layer of vegetation. In the case of bare soil and soil covered with a layer of non-transpiring vegetation, the near-surface soil moisture content was inferred from the soil thermal inertia, which was evaluated by inverting a harmonic soil temperature function. For soil covered with a layer of non-transpiring vegetation, the only difference to that of the approach described above, was that the vegetation was considered as an insulating layer in the soil temperature model. In the case of soil with a transpiring vegetation cover, root-zone soil moisture content was inferred from its relation to vegetation water stress. By relating surface temperature to evapotranspiration rate, the vegetation

water stress was evaluated, using a relationship between evapotranspiration rate, vapour pressure deficit, vegetation type and vegetation water stress.

Ottlé and Vidal-Madjar (1994) have used a similar approach to infer near-surface soil moisture content using thermal infra-red observations. In this instance, the soil moisture content was inferred by inverting a one-dimensional **Soil-Vegetation-Atmosphere-Transfer** (SVAT) model using thermal infra-red observations of surface temperature. The SVAT model used by Ottlé and Vidal-Madjar (1994) calculated the surface fluxes, surface temperature and near-surface soil moisture content by solving simultaneously the energy budget equation on the bare soil surface and that above the canopy. The thermal and hydraulic transfers were described by three important parameters: thermal inertia, hydraulic diffusivity and evaporation. Atmospheric data necessary to run the model were daily variation in incoming radiation, air temperature, humidity and the 2 m wind speed. The three key vegetation parameters of the SVAT model were the height of the vegetation, minimum leaf resistance to evaporation and the **Leaf Area Index (LAI)**.

The spectral properties of leaves, and particularly of chlorophyll, lead to vegetation having a low reflectance in the visible range and a high reflectance in the near infra-red range. Therefore a combination of these two reflectances is a good indicator of vegetation properties. The **Normalised Difference Vegetation Index (NDVI)** is determined from the reflectance levels in both the near infra-red (a_{nir}) and a visible (a_{vis}) waveband, by the relationship

$$NDVI = \frac{a_{nir} - a_{vis}}{a_{nir} + a_{vis}} \quad (2.10).$$

The vegetation fractional cover fc can be deduced from the study of yearly variation of this index using

$$fc = \frac{NDVI - NDVI_{\min}}{NDVI_{\max} - NDVI_{\min}} \quad (2.11),$$

where $NDVI_{min}$ and $NDVI_{max}$ are the minimum and maximum values observed during the whole vegetative period.

In the study by Ottlé and Vidal-Madjar (1994) for inferring near-surface soil moisture content, LAI was estimated by a relationship with fc , and the height of vegetation was estimated from a relationship with LAI . To invert the SVAT model for near-surface soil moisture content, the SVAT model was run with different soil moisture values until the difference between the modelled and observed surface temperatures was less than 1.5 K.

As surface radiant temperature depends on the soil moisture content and the distribution of vegetation, Gillies and Carlson (1995) developed a method for determining near-surface soil moisture availability (M_o), using a physical relationship between NDVI and surface radiant temperature. While the surface radiant temperature was inferred directly from the thermal infra-red observations, NDVI is determined from the reflectance levels in both the near infra-red and a visible waveband, by the relationship in (2.10). When NDVI was plotted against surface radiant temperature, a warm edge was said to exist when the warm side of the distribution in the scatterplot was both sharply defined and smoothly varying, as shown in Figure 2.12. This warm edge represented the zero soil moisture content for varying proportions of vegetation cover. The rounded top to the distribution was due to maximum reflection from the 100% vegetation cover, while the relatively wide and flat base of the distribution corresponded to sunlit bare soil.

Once the 0% and 100% vegetation cover limits were evaluated, and the 0% moisture availability line defined, running simulations in the SVAT model for varying fc amounts allowed for determination of a relationship between NDVI and fc . Likewise, simulations in the SVAT model over the theoretical range of soil moisture availability (0 - 1.0) within the full range of fractional vegetation cover yielded a relationship for soil moisture availability at any surface radiant temperature and NDVI, as indicated in Figure 2.12.

A limitation of this method for determining soil moisture availability is that the truncated vertex of the “triangle” constitutes a zone in which isopleths of M_o converge. This is due to the fact that most of the soil is obscured at high fc .

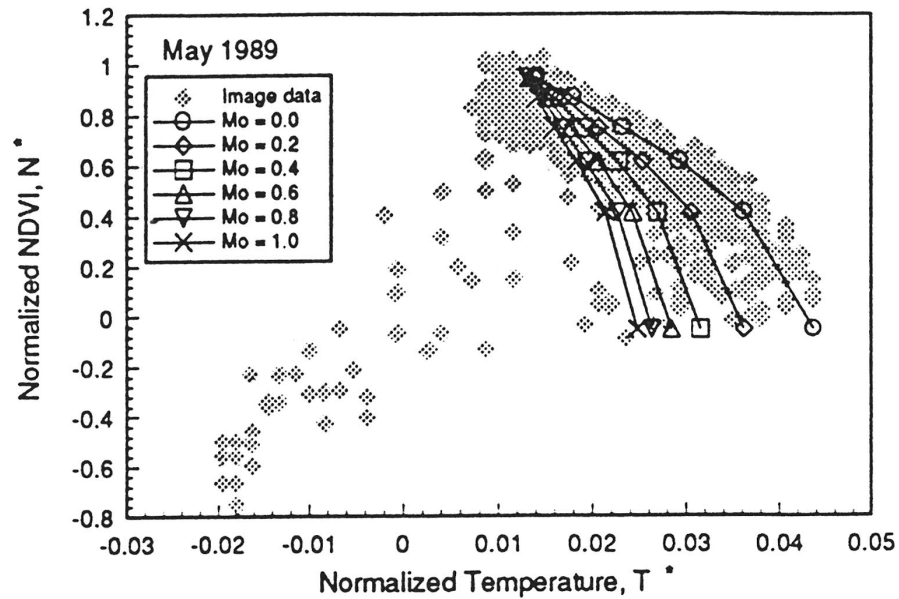


Figure 2.12: Normalised NDVI versus normalised temperature, with isopleths of near-surface soil moisture availability overlaid (Gillies and Carlson, 1995).

Thus, the upper part of the triangle is an area where the errors in the inferred soil moisture content will be largest. Therefore, Gillies and Carlson (1995) suggest that reliable results may be obtained by limiting evaluation of M_o to the range of fractional vegetation cover from 0 to 80%.

2.4.3 MICROWAVE REMOTE SENSING

Microwave remote sensing measures the electromagnetic radiation in the microwave region of the electromagnetic spectrum, which has wavelengths between 0.5 and 100 cm. This region is subdivided into bands, which are often referred to by a lettering system (Table 2.2). However, for remote sensing in the microwave region, only wavelengths greater than about 5 cm are particularly effective, as they have fewer problems with the atmosphere and vegetation, sense a deeper soil layer, and maximise soil moisture sensitivity (Schmugge, 1985; Jackson *et al.*, 1996).

The difference between passive and active microwave remote sensing is the source of the electromagnetic energy. All matter at temperatures above absolute zero emits electromagnetic radiation due to the motion of the charged particles of its atoms and molecules (de Troch *et al.*, 1996). Passive microwave remote sensing measures this naturally emitted radiation from the earth in the

Table 2.2: Microwave band designations (Lillesand and Kiefer, 1994).

Band Designation	Wavelength (cm)	Frequency (GHz)
K _a	0.75 – 1.10	40.0 – 26.5
K	1.10 – 1.67	26.5 – 18.0
K _u	1.67 – 2.40	18.0 – 12.5
X	2.40 – 3.75	12.5 – 8.0
C	3.75 – 7.50	8.0 – 4.0
S	7.50 – 15.0	4.0 – 2.0
L	15.0 – 30.0	2.0 – 1.0
P	30.0 – 100	1.0 – 0.3

microwave region of the electromagnetic spectrum. In contrast, active microwave remote sensing, otherwise known as radar, sends out a pulse of electromagnetic radiation and measures the amount that is scattered back in the direction of the sensor (Jackson *et al.*, 1996), defined as the average scattering cross-section per unit area (de Troch *et al.*, 1996).

The fundamental basis of microwave remote sensing for soil moisture content is the contrast in dielectric properties of water and dry soil, and the relationship between the Fresnel reflection coefficient and dielectric constant. By assuming that the target being observed is a plane surface with surface geometric variations and volume discontinuities much smaller than the wavelength, only refraction and absorption of the media need to be considered. Thus, the Fresnel reflection equations predict the surface reflectivity as a function of the refractive index (related to the ratio of the dielectric constants of the two media) of the target and the viewing angle, based on the polarisation of the sensor. For a land surface, the target consists of the interface between air and soil. Since the dielectric constant of the air is a known value, the reflectivity provides a measurement of the dielectric constant of the soil medium (Jackson *et al.*, 1996).

The main advantage of microwave remote sensing over remote sensing in the visible and infra-red regions, is the effect of atmospheric gases and clouds on the attenuation of the signal received by the sensor. The attenuation by atmospheric gases, and in particular clouds, is significant for radiation in the high frequency (short wavelength) region of the electromagnetic spectrum. However, the attenuation is negligible for frequencies below 10 GHz (wavelength above

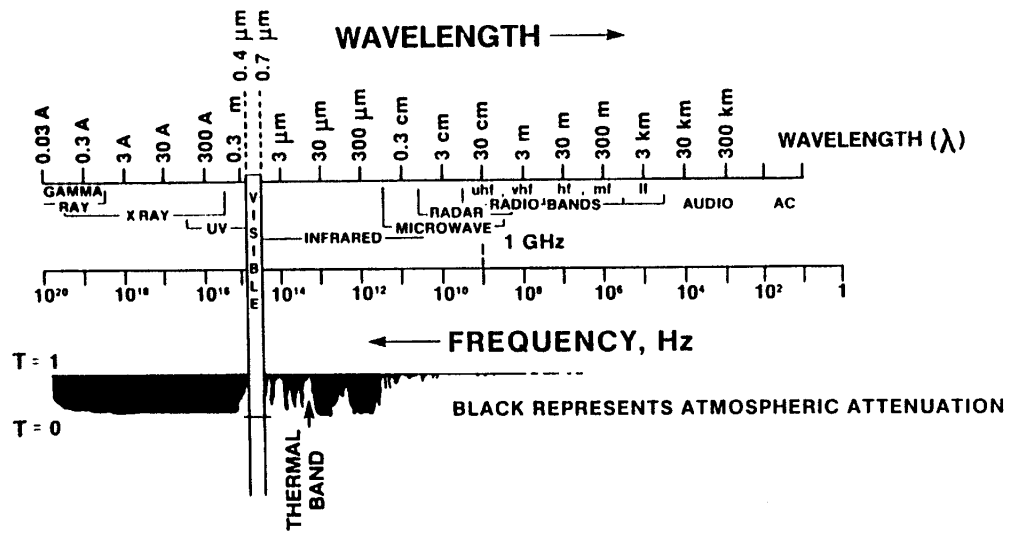


Figure 2.13: Schematic representation of the electromagnetic spectrum on a logarithmic scale. The bottom half of this figure shows atmospheric transmissivity as a function of frequency (Schmugge, 1985).

3 cm). Clouds of ice particles also have a negligible effect on microwave radiation due to small particle sizes and the low dielectric constant of ice. The effects of non-raining clouds on microwave radiation are negligible for frequencies below about 15 GHz, but the effects of raining clouds are only negligible if frequencies are below 3 GHz (Schmugge, 1985). The placement of microwaves in the electromagnetic spectrum is shown in Figure 2.13. By looking at the atmospheric transmissivity (transmissivity = 1 – attenuation) at the bottom of this figure, the advantage of microwave wavelengths for remote sensing becomes obvious. Another unique advantage of microwave remote sensing is that vegetation is semi-transparent at longer microwave wavelengths (Jackson and Schmugge, 1991). Microwave measurements are also independent of solar illumination and can be made at any time of the day (Jackson *et al.*, 1996).

One important difference between active and passive microwave remote sensing systems is the resolution of the resulting data. Active sensors have the capability to provide high spatial resolution (on the order of tens of metres) but are more sensitive to surface roughness, topographic features and vegetation than passive systems. On the other hand, the passive systems can only provide spatial resolutions on the order of tens of kilometres and may be as large as 100 km. Therefore, consideration must be given to how the data will be used. If the soil moisture data is for meteorological and climate models with a low spatial

Table 2.3: Comparison of passive and active microwave remote sensing (Engman, 1992).

Characteristic	Passive Microwave	Active Microwave
Signal to Noise	good – very good	fair – good
Data Rate	low	very high
Spatial Resolution	10 – 100 km	10 m
Swath Width	wide	narrow – moderate
Vegetation Effect	moderate – serious	moderate
Roughness Effect	slight	serious
Topographic Effect	slight	serious
Revisit Time	good	poor – moderate

resolution, passive systems may be appropriate. However, if the soil moisture data is for detailed hydrologic process studies and partial area hydrology, the passive data would appear of little use (Engman, 1990; Engman and Chauhan, 1995), requiring spatial resolutions on the order of 10 m or less (van de Griend and Engman, 1985). It has also been noted by Ulaby *et al.* (1978) that it is difficult to provide a reliable measurement of soil moisture content from a sensor with a resolution cell of the size obtained from passive microwave sensors, unless the terrain is free from lakes and cultural features. A comparison of passive and active microwave systems is made in Table 2.3.

To account for the low resolution of passive microwave sensors, Kumar (1999) has recently proposed a technique for relating the large passive microwave footprint to the small scale variability in soil moisture content through a tree structure arrangement and a multiple scale Kalman-filtering algorithm. This technique utilises a state-space model that relates the soil moisture content with the underlying soil hydrologic properties by a fractal process.

2.4.4 PASSIVE MICROWAVE REMOTE SENSING

Passive microwave radiometric measurements in the 1 to 10 GHz range (L- to X-Band) are recognised to be of the greatest utility in measuring soil moisture content. However, L-Band radiation is considered to yield the most accurate results over the widest range of conditions (Entekhabi *et al.*, 1994), as roughness and heterogeneity effects and attenuation by the atmosphere and vegetation are minimised (Galantowicz *et al.*, 1999). Accurate soil moisture

measurements are limited to regions that have either bare soil or low to moderate amounts of vegetation cover (Njoku and Entekhabi, 1996).

A microwave radiometer measures the self emitted and/or reflected radiation from the earth's surface in the microwave region of the electromagnetic spectrum, whose intensity is characterised by the brightness temperature T_b , which is often referred to as the radio-brightness. The amount of energy generated at any point within the soil volume depends on the soil dielectric properties and the soil temperature at that point. Hence, the brightness temperature is highly variable during the course of the day, as the depth of soil which actually contributes to T_b is quite shallow (Jackson, 1997).

As the energy propagates upward through the soil, it is affected by the dielectric gradient along the path of propagation. In addition, as the energy crosses the surface boundary, it is reduced by the effective transmission coefficient (emissivity), which is determined by the dielectric characteristics of the near-surface soil (Schmugge *et al.*, 1980). The variation in soil emissivity in the microwave region is rather weak, with a range from about 0.95 for dry soil (5% v/v) to 0.6 or less for wet soil (40% v/v) (Schmugge, 1985; Jackson *et al.*, 1996; Njoku and Entekhabi, 1996). However, for soil at a temperature of 300 K, this variation in emissivity corresponds to a brightness temperature variation of 90 K, which is much larger than the noise sensitivity threshold of a microwave radiometer, being typically less than 1 K (Njoku and Entekhabi, 1996).

2.4.4.1 **Brightness Temperature Models**

Brightness temperature is dependent on both the soil moisture and temperature profiles of the soil, and is essentially the product of soil temperature and emissivity at the soil surface through the Rayleigh-Jeans approximation to Plank's law (Jackson *et al.*, 1981; Schmugge, 1985). By this relationship, the value of T_b measured by a radiometer above a surface is given by

$$T_{b_p} = \tau(\Gamma_p T_{sky} + e_p T_{soil}) + T_{atm} \quad (2.12),$$

where Γ_p is the surface reflectivity for polarisation p , e_p is the surface emissivity for polarisation p and τ is the atmospheric transmission. The first right hand side term in this relationship is the reflected sky brightness temperature, which depends on the wavelength and atmospheric conditions. The second term is the emission from the soil and the third term is the contribution from the atmosphere between the surface and the receiver (Jackson *et al.*, 1981; Schmugge, 1985).

For typical remote sensing applications using longer wavelengths (greater than 5 cm), the atmospheric transmission approaches 99%. Furthermore, the atmospheric T_{atm} and sky T_{sky} contributions are both less than 5 K, each of which is small compared to the soil contribution (Engman and Chauhan, 1995). Thus, by neglecting these two terms the Rayleigh approximation may be simplified to

$$T_{b_p} = e_p T_{soil} = (1 - \Gamma_p) T_{soil} = \left(1 - |R_p|^2\right) T_{soil} \quad (2.13),$$

where Kirchoff's reciprocity theorem relates the emissivity to the reflectivity by $e_p = 1 - \Gamma_p$, with $\Gamma_p = |R_p|^2$ being the reflectivity for polarisation p and R_p being the reflection coefficient for polarisation p . Although the relationship between emissivity and brightness temperature is linear, there is a non-linear dependence on the soil moisture content, because the reflection coefficient of the soil is related in a non-linear way to the dielectric constant of the soil (Engman and Chauhan, 1995). The microwave emission from the soil has generally been predicted by the Fresnel equations (Jackson *et al.*, 1987; Galantowicz *et al.*, 1999), as given in (2.14a) for horizontal polarisation and (2.14b) for vertical polarisation.

$$e_h = 1 - \left| \frac{\cos \vartheta - \sqrt{\epsilon_r - \sin^2 \vartheta}}{\cos \vartheta + \sqrt{\epsilon_r - \sin^2 \vartheta}} \right|^2 \quad (2.14a)$$

$$e_v = 1 - \left| \frac{\epsilon_r \cos \vartheta - \sqrt{\epsilon_r - \sin^2 \vartheta}}{\epsilon_r \cos \vartheta + \sqrt{\epsilon_r - \sin^2 \vartheta}} \right|^2 \quad (2.14b),$$

where ϑ is the look angle for the instrument measured from nadir (degrees), and ϵ_r is the relative dielectric constant of the soil.

The majority of brightness temperature models presented in the literature are based on the simplified Rayleigh approximation given in (2.13), and are easily invertible for soil moisture content. These models consist of two types, being the emissivity and radiative transfer models, and differ only in their treatment of T_{soil} (Galantowicz *et al.*, 1999).

The emissivity model assumes a grey body approximation by assigning a constant soil temperature with depth (Galantowicz *et al.*, 1999), which can lead to errors in regions where the diurnal soil surface temperature variations are large (Njoku and Kong, 1977). The temperature and moisture contents of soils exhibit natural variability as a function of depth. Therefore it is not strictly correct to represent soil brightness temperature and emissivity by such approximations, especially at longer wavelengths, which may respond to soil moisture and temperature conditions over depths of several centimetres (Njoku and Entekhabi, 1996).

Current radiative transfer models consist of the conventional radiative transfer and the gradient radiative transfer, which impose a varying soil temperature profile. The conventional radiative transfer determines T_{soil} by integrating soil temperature over the soil profile, where each soil layers contribution to T_{soil} is a function of a local extinction coefficient and the optical distance to the soil surface. The gradient radiative transfer model is an approximation of the conventional radiative transfer model, by taking T_{soil} as a linear function of depth, and the extinction coefficient as a constant (Galantowicz *et al.*, 1999). In cases where the sub-surface dielectric properties vary rapidly with respect to wavelength in the medium, radiative transfer models become inaccurate and the brightness temperature must be modelled using a coherent electromagnetic wave approach (Njoku and Kong, 1977). A coherent wave treatment is necessary to interpret the effects of sharp discontinuities in the soil moisture profile (Njoku and Entekhabi, 1996).

Other approaches for direct modelling of the brightness temperature assume complete knowledge of the soil temperature and moisture profiles, and are

not easily invertible. These models are based on both coherent wave theory and non-coherent radiative transfer (Galantowicz *et al.*, 1999). Coherent wave transfer models account for both the amplitude and phases of the electromagnetic fields within the medium (Ulaby *et al.*, 1981), and the boundary conditions on the electric fields across layer boundaries are used to calculate the radiation intensity (Schmugge and Choudhury, 1981). The incoherent approach relies on amplitudes only (Ulaby *et al.*, 1981), and the transfer of energy between layers is determined by the reflectivity calculated from the Fresnel equations. To evaluate the intensity of radiation within the soil using a coherent model, the electromagnetic field vectors must be calculated from a solution to Maxwell's equations (Schmugge and Choudhury, 1981).

The coherent stratified medium approach of Njoku and Kong (1977) takes into account both non-uniform temperature and rapidly varying moisture profiles of the soil, and has been presented as a summation over the entire depth of the soil column. The soil discretisation used by this model is given in Figure 2.14, and the

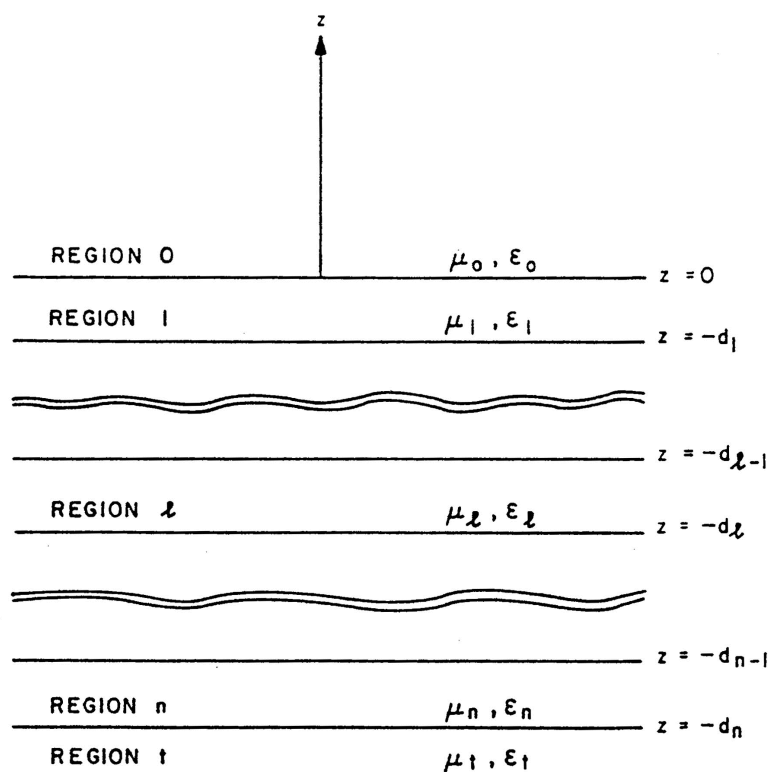


Figure 2.14: Geometrical configuration used for evaluation of brightness temperature from a coherent stratified medium (Tsang *et al.*, 1975).

equations used for evaluating brightness temperature for h and v polarisation are given in (2.15a) and (2.15b) respectively.

$$T_{b_h} = \frac{k_o}{\cos \vartheta} \sum_{l=1}^N \left\{ \frac{\varepsilon_l'' T_l}{\varepsilon_o} \left[\begin{array}{l} \frac{|A_l \exp(-ik_{z_l} d_l)|^2}{2k_{z_l}''} \{1 - \exp[2k_{z_l}''(d_{l-1} - d_l)] - \\ \frac{|B_l \exp(ik_{z_l} d_l)|^2}{2k_{z_l}''} \{1 - \exp[-2k_{z_l}''(d_{l-1} - d_l)] - \\ \frac{[A_l \exp(-ik_{z_l} d_l)][B_l \exp(ik_{z_l} d_l)]}{2ik_{z_l}'} \{1 - \exp[-i2k_{z_l}'(d_{l-1} - d_l)] + \\ \frac{[A_l \exp(-ik_{z_l} d_l)][B_l \exp(ik_{z_l} d_l)]}{2ik_{z_l}'} \{1 - \exp[i2k_{z_l}'(d_{l-1} - d_l)] \} \end{array} \right] \right\} \quad (2.15a)$$

$$+ \frac{k_o}{\cos \vartheta} \frac{\varepsilon_l'' T_l}{\varepsilon_o} \frac{|T_h|^2 \exp(-2k_{z_l}'' d_n)}{2k_{z_l}''}$$

$$T_{b_v} = \frac{k_o}{\cos \vartheta} \sum_{l=1}^N \left\{ \frac{\varepsilon_l'' T_l}{\varepsilon_o |k_l|^2} \left(|k_{z_l}|^2 + k_{x_o}^2 \right) \left[\begin{array}{l} \frac{|C_l \exp(-ik_{z_l} d_l)|^2}{2k_{z_l}''} \{1 - \exp[2k_{z_l}''(d_{l-1} - d_l)] - \\ \frac{|D_l \exp(ik_{z_l} d_l)|^2}{2k_{z_l}''} \{1 - \exp[-2k_{z_l}''(d_{l-1} - d_l)] + \\ \frac{[C_l \exp(-ik_{z_l} d_l)][D_l \exp(ik_{z_l} d_l)]}{2ik_{z_l}'} \times \\ \frac{|k_{z_l}|^2 - k_{x_o}^2}{|k_{z_l}|^2 + k_{x_o}^2} \{1 - \exp[-i2k_{z_l}'(d_{l-1} - d_l)] - \\ \frac{[C_l \exp(-ik_{z_l} d_l)][D_l \exp(ik_{z_l} d_l)]}{2ik_{z_l}'} \times \\ \{1 - \exp[i2k_{z_l}'(d_{l-1} - d_l)] \} \end{array} \right] \right\} \quad (2.15b)$$

$$+ \frac{k_o}{\cos \vartheta} \frac{\varepsilon_l'' (|k_{z_l}|^2 + k_x^2) T_l}{\varepsilon_o |k_l|^2} \frac{|T_v|^2 \exp(-2k_{z_l}'' d_n)}{2k_{z_l}''}$$

The subscripts l refer to the quantities in the l th layer of the medium, and d_l is the depth below the surface of the soil to the interface between the l th and $(l+1)$ th layer. The subscript o refers to the free space values, and the subscript t refers to the region extending beyond the last layer, while ' and '' refer to the real and imaginary parts of the variable respectively. T is the soil temperature and k is the wave number given by $k = 2\pi/\lambda = 2\pi f \sqrt{\mu\varepsilon}$, where f is the frequency, μ is the magnetic permeability and $\varepsilon = \varepsilon' + i\varepsilon''$ is the dielectric constant. k_x is the x component of the wave number given by $k_x = k \sin \vartheta$, and k_z is the z component given by $k_z = k \cos \vartheta$, where ϑ is the instrument look angle. The A_l , B_l , C_l , D_l , T_h and T_v are wave amplitudes and are related to one another by the propagation matrices given in Kong (1975), which are reproduced below.

$$\begin{bmatrix} A_{l+1} e^{-ik_{z(l+1)} d_{l+1}} \\ B_{l+1} e^{ik_{z(l+1)} d_{l+1}} \end{bmatrix} = \frac{1}{2} \left(1 + \frac{\mu_{l+1} k_{zl}}{\mu_l k_{z(l+1)}} \right) \cdot \begin{bmatrix} \exp(-ik_{z(l+1)}(d_{l+1} - d_l)) & R_{h(l+1)l} \exp(-ik_{z(l+1)}(d_{l+1} - d_l)) \\ R_{h(l+1)l} \exp(ik_{z(l+1)}(d_{l+1} - d_l)) & \exp(ik_{z(l+1)}(d_{l+1} - d_l)) \end{bmatrix} \cdot \begin{bmatrix} A_l \exp(-ik_{zl} d_l) \\ B_l \exp(ik_{zl} d_l) \end{bmatrix} \quad (2.16a)$$

$$\begin{bmatrix} C_{l+1} e^{-ik_{z(l+1)} d_{l+1}} \\ D_{l+1} e^{ik_{z(l+1)} d_{l+1}} \end{bmatrix} = \frac{1}{2} \left(1 + \frac{\mu_{l+1} k_{zl}}{\mu_l k_{z(l+1)}} \right) \cdot \begin{bmatrix} \exp(-ik_{z(l+1)}(d_{l+1} - d_l)) & R_{v(l+1)l} \exp(-ik_{z(l+1)}(d_{l+1} - d_l)) \\ R_{v(l+1)l} \exp(ik_{z(l+1)}(d_{l+1} - d_l)) & \exp(ik_{z(l+1)}(d_{l+1} - d_l)) \end{bmatrix} \cdot \begin{bmatrix} C_l \exp(-ik_{zl} d_l) \\ D_l \exp(ik_{zl} d_l) \end{bmatrix} \quad (2.16b)$$

$$R_{h(l+1)l} = - \left(\frac{1 - \left(\frac{\mu_l k_{z(l+1)}}{\mu_{l+1} k_{zl}} \right)}{1 + \left(\frac{\mu_l k_{z(l+1)}}{\mu_{l+1} k_{zl}} \right)} \right) \quad (2.17a)$$

$$R_{v(l+1)l} = - \left(\frac{1 - \left(\frac{\varepsilon_l k_{z(l+1)}}{\varepsilon_{l+1} k_{zl}} \right)}{1 + \left(\frac{\varepsilon_l k_{z(l+1)}}{\varepsilon_{l+1} k_{zl}} \right)} \right) \quad (2.17b)$$

$$T_h = \frac{2}{1 + \left(\frac{\mu_l k_{z(l+1)}}{\mu_{l+1} k_{zl}} \right)} \quad (2.18a)$$

$$T_v = \frac{2}{1 + \left(\frac{\varepsilon_l k_{z(l+1)}}{\varepsilon_{l+1} k_{zl}} \right)} \quad (2.18b)$$

A question surrounding the evaluation of stratified models is the layer thickness and depth of soil that should be used. Raju *et al.*, (1995) found that if the layer thickness is larger than 0.1 cm in the stratified coherent model of Wilheit

(1978), the computed brightness temperature differs significantly to that computed with very thin layers. Therefore, they suggest that the layer thickness should not exceed 0.01 cm if the difference in simulated brightness temperature is not to exceed 1 K. Raju *et al.* (1995) also found that the soil depth to be used in the model should be between one-tenth of the wavelength and the wavelength, if the brightness temperature is not to be affected by more than 1 K.

The stratified coherent model of Wilheit (1978) is simpler than that of Njoku and Kong (1977) and uses a solution of the Maxwell's equations and the boundary conditions at the interfaces, to calculate the electric field in each layer. These electric field values are used to calculate the energy fluxes, and thus obtain the fractional absorption f_{p_l} in each layer l . If T_l is the thermodynamic temperature in the l th layer of the N dielectrically homogeneous layers in the air-soil system, the layer radiates energy equal to the product of the fractional absorption and the soil temperature. Applying the Rayleigh-Jeans approximation to Plank's law, brightness temperature for polarisation p (T_{b_p}) is written as

$$T_{b_p} = \sum_{l=2}^N f_{p_l} T_l + R_p T_{sky} \quad (2.19a)$$

$$\sum_{l=2}^N f_{p_l} = e_p \quad (2.19b),$$

where R_p is the reflectivity for the radiation incident on the air-soil interface for polarisation p and T_{sky} is the brightness temperature equivalent of sky and atmospheric radiation incident on the soil (Wang *et al.*, 1983).

As detailed information about the soil temperature profile is not generally available for inversion of brightness temperature measurements for soil moisture content, Choudhury *et al.* (1982) have proposed a method for estimating an effective soil temperature by using only surface and deep soil temperatures.

$$T_{eff} = T_{\infty} + a(T_{surf} - T_{\infty}) \quad (2.20),$$

where T_{eff} is the effective soil temperature, T_{surf} is the soil surface temperature, T_{∞} is the deep soil temperature and a is an empirically determined constant; given as 0.802, 0.667, 0.480, 0.246 and 0.084 for wavelengths of 2.8, 6.0, 11.0, 21.0 and 49.0 cm respectively (Choudhury *et al.*, 1982). Choudhury *et al.* (1982) suggest that the surface temperature may be estimated from thermal infra-red observations, or meteorological data of near-surface air temperature, while the deep soil temperature can be modelled based on geographic location and season.

The major problem with the above brightness temperature models is that the passive microwave response of the soil is affected not only by the soil moisture and temperature profile variations, but also by the surface roughness, and vegetation cover (Njoku and Kong, 1977). Various researchers have made attempts to quantify the effects of surface roughness and vegetation on the brightness temperature, and have presented models to account for these effects. However, it has been shown by Wang *et al.* (1987) that microwave emission is less affected by surface roughness than by vegetation.

2.4.4.2 Roughness Effects

Field measurements made by Newton and Rouse (1980) and Wang *et al.* (1983) have indicated that roughening of the soil surface increases soil emissivity and decreases the sensitivity to soil moisture content, thus reducing the range of T_b from wet to dry soils (van de Griend and Engman, 1985). This increase in emissivity can be attributed to the increase in soil surface area that interfaces with the air, and thus transmits the upwelling energy (Schmugge, 1985). Newton *et al.* (1983) have noted that the effects of surface roughness decrease as the wavelength increases.

To account for the effects of surface roughness on soil emissivity, Choudhury *et al.* (1979) have presented a modification to the emissivity of a smooth surface as

$$e_{R_p} = 1 - \left[(1 - e_p) \exp(-h \cos^2 \vartheta) \right] \quad (2.21a)$$

$$h \approx 4\sigma^2 \left(\frac{2\pi}{\lambda_o} \right)^2 \quad (2.21b),$$

where h is an effective roughness parameter, σ is the standard deviation of surface roughness (cm), λ_o is the free space wavelength (cm), ϑ is the viewing angle (degrees), and e_p and e_{R_p} are the smooth and rough surface emissivity respectively for a given polarisation p . The parameter h has been shown to be loosely correlated with the standard deviation of the surface heights (2.21b), although no exact functional relationship has been established. For smoother surfaces such as stubble, pastures and wheat, a typical value of h is 0.1, and for very rough fields such as those recently tilled, a value of h equal to 0.5 is typical (Choudhury, *et al.*, 1979; Wang *et al.*, 1983).

Wang *et al.* (1983) have proposed a more general variation of (2.21a), by adding a polarisation mixing factor Q . The rough surface emissivities for horizontal and vertical polarisations are given as

$$e_{R_h} = 1 - [(1 - Q)(1 - e_h) + Q(1 - e_v)] \exp[-hG(\vartheta)] \quad (2.22a)$$

$$e_{R_v} = 1 - [(1 - Q)(1 - e_v) + Q(1 - e_h)] \exp[-hG(\vartheta)] \quad (2.22b),$$

where e_h and e_v are the smooth surface emissivities for horizontal and vertical polarisations respectively and h is the effective roughness parameter. Wang *et al.* (1983) found that measured and calculated brightness temperatures could not be matched with $G(\vartheta) = \cos^2 \vartheta$, as used by Choudhury *et al.* (1979), but found agreement for $G(\vartheta) \cong 1$.

2.4.4.3 Vegetation Effects

The influence of vegetation on the brightness temperature measured by the radiometer is the result of absorption and re-emission (Schmugge, 1985; Engman and Chauhan, 1985), with the effect of reducing measurement sensitivity (van de Griend and Engman, 1985). This occurs through the vegetation absorbing some of the radiation coming up from the soil and emitting radiation itself. Hence, for a

sufficiently thick layer of vegetation, only the radiation from the vegetation itself is observed (Schmugge, 1985). The effects from scattering within the vegetation canopy are most significant at frequencies higher than 5 to 10 GHz (Wigneron *et al.*, 1998).

Jackson *et al.* (1982) have shown that absorption by vegetation can be quantified in terms of the water content of the vegetation, whilst Schmugge *et al.* (1988) have demonstrated that dead vegetation can have an attenuating effect on the microwave emission from soil. It has also been noted (Newton and Rouse, 1980; Jackson *et al.*, 1982; Engman and Chauhan, 1995) that vegetation effects are a function of the free space wavelength, with vegetation canopies being more transparent for longer wavelengths than for shorter wavelengths. Newton and Rouse (1980) suggest that dense vegetation to a height of 125 cm has little effect on the measured emission at 21.4 cm wavelength for incident angles below 35°, while at 2.8 cm wavelength the soil emission is completely masked. Furthermore, the effect of vegetation is more significant as the vegetation water content is increased (Jackson and Schmugge, 1991).

A vegetation canopy absorbs the emission from the soil and adds to the total radiative flux with its own emission, assuming scattering is negligible. A model of this process, which treats the problem as a two-layer incoherent medium, is described by (Ulaby *et al.*, 1986)

$$T_{b_p} = [1 + (1 - e_p) \Upsilon_{veg} (1 - \Upsilon_{veg}) (1 - \alpha) T_{veg} + (e_p \Upsilon_{veg} T_{soil})] \quad (2.23),$$

where e_p is the emissivity of the smooth soil surface at polarisation p , α is the single scattering albedo of the vegetation, Υ_{veg} is the transmissivity of the vegetation layer, T_{veg} is the physical temperature of the vegetation (K) and T_{soil} is the physical temperature of the soil (K). At microwave wavelengths the single scattering albedo term is almost zero, varying between 0.05 and 0.10 (Jackson and Schmugge, 1991). Chanzy *et al.* (1997) have shown that the single scattering albedo can be neglected at C-Band when the amount of vegetation is low. Thus, by assuming that α equals zero, which may be questionable at wavelengths shorter than 5 cm (Jackson and Schmugge, 1991), and that the physical

temperature of the vegetation and the soil are the same with value T_{surf} , Jackson and Schmugge (1991) have reduced (2.23) to

$$T_{b_p} = [1 - (1 - e_p) \Upsilon_{veg}^2] T_{surf} \quad (2.24),$$

where T_{surf} is the surface temperature (K) estimated from thermal infra-red observations under clear sky conditions or meteorological estimates of the air temperature under cloudy conditions (Jackson and Schmugge, 1991), and e_p is the emissivity for polarisation p .

The transmissivity of the attenuating vegetation layer has been described through a relationship with the one-way canopy absorption factor, otherwise known as optical depth τ , which is dependent on the vegetation dielectric properties, plant shape and structure, wavelength, polarisation and look angle. This relationship for vegetation transmissivity is given by

$$\Upsilon_{veg} = \exp[-\tau \sec \vartheta] \quad (2.25),$$

where ϑ is the observation angle (degrees) measured from nadir.

In order to invert (2.24) for the soil moisture content, an estimate of the optical depth is required. Various theoretical and empirical relationships have been proposed for the optical depth (Jackson *et al.*, 1982). A simple theoretical expression for the vegetation optical depth is (Njoku and Entekhabi, 1996)

$$\tau = \frac{Af\theta_{veg} \epsilon''_{veg}}{\cos \vartheta} \quad (2.26),$$

where A is a structure parameter related to the geometry of the vegetation, f is the observation frequency (Hz), θ_{veg} is the water content of the vegetation (kg m^{-2}) and ϵ''_{veg} is the imaginary part of the dielectric constant of the vegetation. The parameter A can be obtained by modelling the vegetation as lossy (conducting) dielectric cylinders or disks in different orientations, but is more commonly estimated empirically for specific vegetation types (Njoku and Entekhabi, 1996).

Alternative relationships for estimating the optical depth have been given as (Ulaby *et al.*, 1986)

$$\tau = 4\pi \left(\frac{d_{veg}}{\lambda_o} \right) \text{Im}(\sqrt{\epsilon_{veg}}) \quad (2.27),$$

and (Schmugge *et al.*, 1988)

$$\tau = \frac{4\pi d_{veg}}{\lambda_o} \sqrt{\frac{\epsilon'_{veg}}{2} \left[\sqrt{1 + \left(\frac{\epsilon''_{veg}}{\epsilon'_{veg}} \right)^2} - 1 \right]} \quad (2.28),$$

where d_{veg} is the thickness of the vegetation layer (cm), λ_o is the free space wavelength (cm), and $\text{Im}(\epsilon_{veg})$ is the imaginary component of the dielectric constant of the vegetation;

An empirical relationship between optical depth and vegetation water content has been given as (Shutko, 1986; Jackson and O'Neill, 1990)

$$\tau = \theta_{veg} b \quad (2.29),$$

where b is a regression parameter unique to the type of vegetation, the free space wavelength and polarisation. Jackson (1993) has presented a plot of b for different wavelengths and vegetation types, as given in Figure 2.15.

An interesting observation of Figure 2.15, excluding the observations for grass, is the small variation of the parameter b in the L-Band range (wavelength 15 to 30 cm). Based on these results, it would appear that a single value of b equal to 0.15 is representative of most agricultural crops, with the exception of grasses (Jackson, 1993).

These relationships for optical depth require an estimate of the vegetation water content. However, previous research has shown that vegetation water content can be estimated using existing sensors and algorithms (Jackson and Schmugge, 1991).

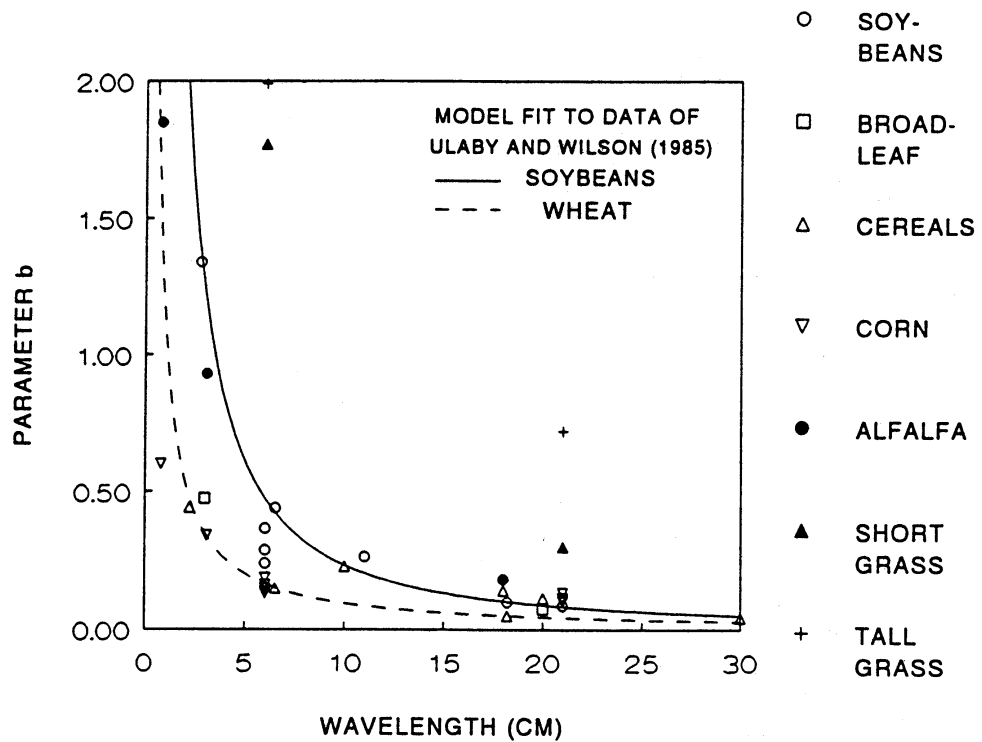


Figure 2.15: Observed values of the effects of vegetation on model parameter b as a function of wavelength (Jackson, 1993).

For small values of optical depth τ , which occur for low vegetation density, (2.23) reduces to $T_{b_p} = e_p T_{soil}$, whereas for large τ , which occurs for dense vegetation, the observed brightness temperature approaches $T_{b_p} = T_{veg}$, resulting in the soil being completely masked by the vegetation (Njoku and Entekhabi, 1996).

2.4.4.4 Combined Roughness and Vegetation Effects

As the brightness temperature models presented above only account for vegetation and roughness effects individually, Jackson (1993) has presented an algorithm for inferring near-surface soil moisture content that incorporates both surface roughness and vegetation effects. In the model of Jackson (1993), the brightness temperature of a vegetated surface is given by (2.24), with the smooth surface emissivity e_p taken as being the rough surface emissivity e_{R_p} , as given by (2.21).

2.4.5 ACTIVE MICROWAVE REMOTE SENSING

Active microwave remote sensing involves the use of a radar antenna (either real or synthetic aperture), which transmits wave pulses and receives a return signal whose intensity varies with the target characteristics. The backscattering coefficient σ^o is used to describe the intensity of this reflected radiation from an object (Schmugge, 1985).

Since the scattering behaviour of a surface is governed by its geometrical and dielectric properties relative to the incident radiation, the variations in backscattering are influenced by soil moisture content, surface roughness, surface cover (vegetation), topography, observation frequency, wave polarisation and incidence angle (Schmugge, 1985; Su *et al.*, 1994). A variation of relative dielectric constant between 3 and 30 (a shift in volumetric moisture content between approximately 2.5% and 50%, depending on frequency and soil texture) causes an 8 to 9 dB rise in backscatter coefficient for vv polarisation. This change in backscattering is almost independent of other parameters, such as incidence angle, frequency and surface roughness (Hoeben *et al.*, 1997). The relationship between backscattering coefficient and dielectric constant is non-linear, having a higher sensitivity at low dielectric values as shown in Figure 2.16.

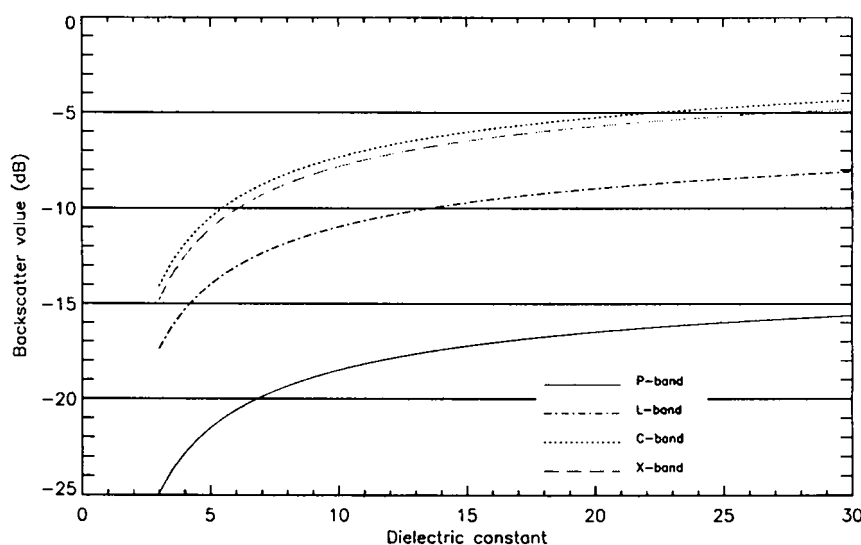


Figure 2.16: Sensitivity of backscattering to dielectric constant at different frequencies: exponential correlation function, $\sigma = 1.4$ cm, $l = 10$ cm, $\theta = 35^\circ$, vv polarisation (Hoeben *et al.*, 1997).

Although surface roughness may not be a serious limitation for passive microwave sensors, at least for most natural surfaces, it is a major limiting factor for active microwave sensors (Wang *et al.*, 1987; Wütherich, 1997) and simple correction procedures are difficult to develop (Jackson *et al.*, 1996). In many cases the effect of roughness may be equal to or greater than the effects of soil moisture content on the backscatter (Autret *et al.*, 1989; Engman and Chauhan, 1995; Altese *et al.*, 1996; Wütherich, 1997), and in ploughed fields, the row structure generated by ploughing presents a periodic pattern that can complicate data interpretation (Beaudoin *et al.*, 1990; Giacomelli *et al.*, 1995). Furthermore, the surface roughness of agricultural fields is not likely to remain constant between overpasses of more than 30 days (Wütherich, 1997) due to reductive tillage and weathering (Beaudoin *et al.*, 1990), or between overpasses on different orbit tracks, which may have large differences in angle with respect to field direction (Wütherich, 1997). However, in contrast to agricultural fields, the surface roughness of natural ecosystems does not change significantly over relatively short time periods (Sano *et al.*, 1998). The dependence of backscatter intensity on surface roughness is represented schematically in Figure 2.17, where an increase of backscattering coefficient with surface roughness is obvious, as reported in experimental studies (eg. Beaudoin *et al.*, 1990).

In general, smooth surfaces behave as specular reflectors and only have strong backscattering at near-zero incidence angles, whereas rough surfaces act as

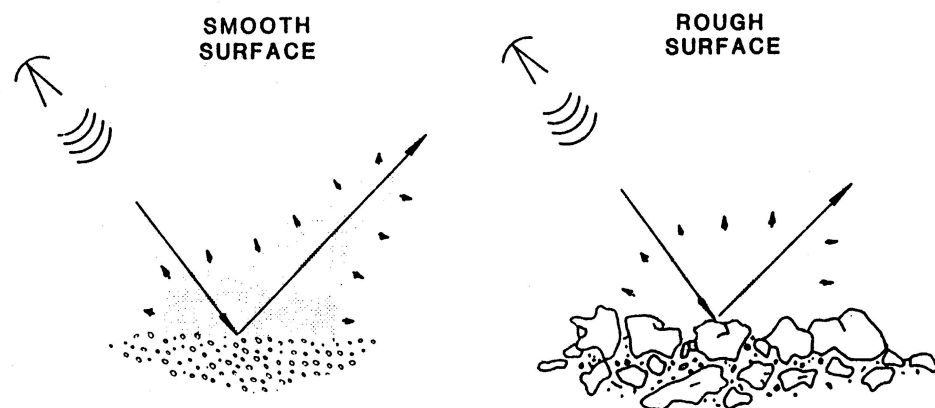


Figure 2.17: Illustration of the effect of surface roughness on backscattering intensity (Schmugge, 1985).

diffuse reflectors with minimal angular variation (Schmugge, 1985). Very rough surfaces are called lambertian reflectors and have no angular variation. As illustrated in Figure 2.18, a surface appears rougher to a shorter wavelength than to a longer wavelength (Brown *et al.*, 1992). Furthermore, for a given wavelength the backscattering from rougher soils is less dependent on the value of the incidence angle (Ulaby *et al.*, 1986).

Several relationships have been proposed for defining the roughness of a

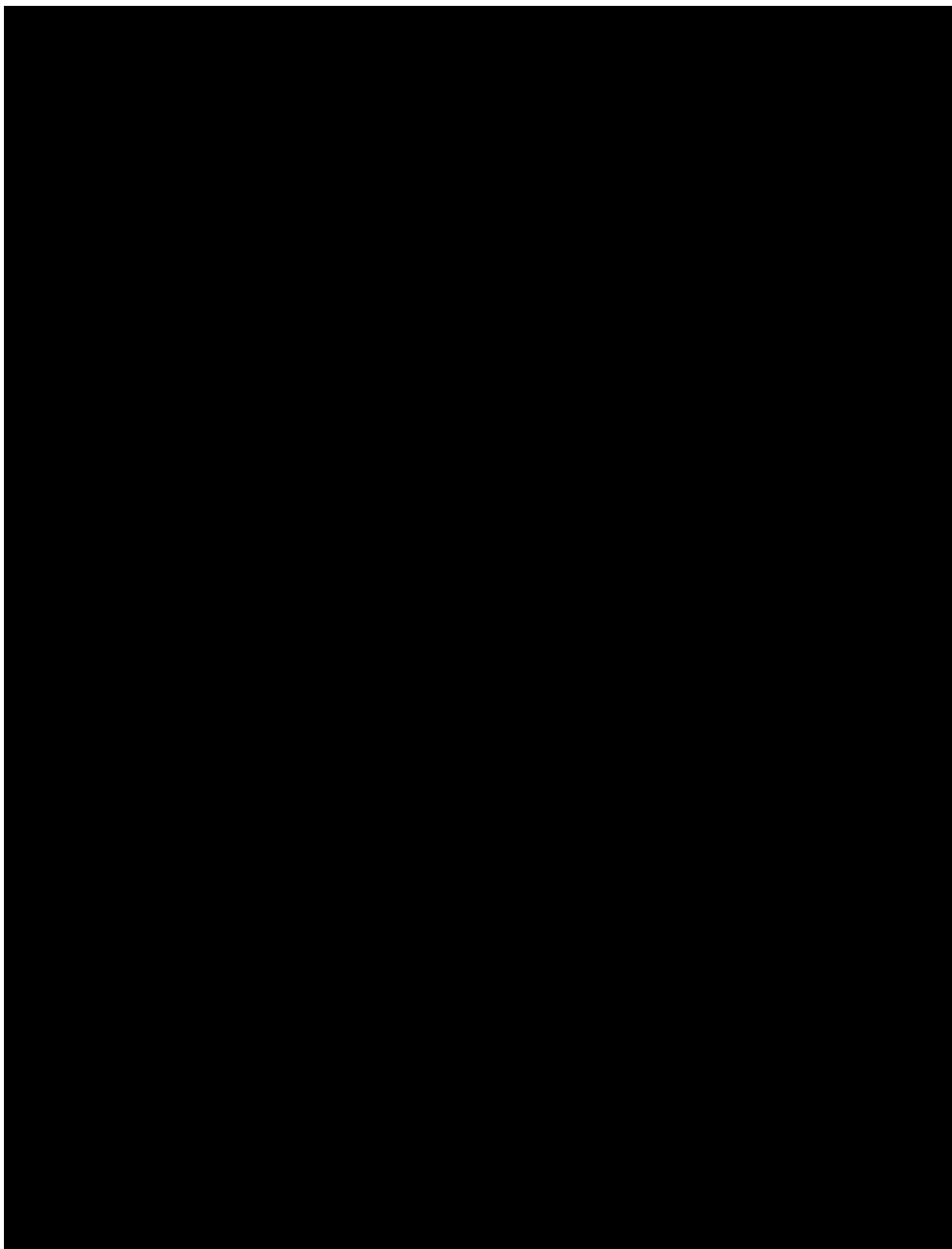


Figure 2.18: Illustration showing the effect of wavelength and surface roughness on the backscattering properties of a surface (Lillesand and Kiefer, 1994).

surface with respect to the wavelength. The Rayleigh criterion states that surfaces can be considered as “rough”, and act as diffuse reflectors if the rms (root mean square) height of the surface variations σ exceeds one-eighth of the wavelength of sensing divided by the cosine of the local incidence angle ($\sigma > \lambda_o/8\cos\vartheta$). Surfaces are considered “smooth” by the Rayleigh criterion, and act as specular reflectors when $\sigma < \lambda_o/8\cos\vartheta$.

As the Rayleigh criterion does not consider that there can be a category of surface variation intermediate between rough and smooth, the Modified Rayleigh criterion is used to define such situations. This criterion considers rough surfaces to be those with $\sigma > \lambda_o/4.4\cos\vartheta$ and smooth where $\sigma < \lambda_o/25\cos\vartheta$. Intermediate values are considered to have intermediate roughness (Lillesand and Kiefer, 1994). Ulaby *et al.* (1982) have proposed an alternative relationship for categorising surfaces as rough or smooth, which is independent of incidence angle. In this relationship, smooth surfaces are defined as having $k_o\sigma < 0.2$ and very rough surfaces as having $k_o\sigma > 1$, where k_o is the free space wave number given by $k_o = 2\pi/\lambda_o$.

As with passive microwave remote sensing, the observations made with active microwave remote sensing are affected by vegetation cover and reduce the sensitivity of the return signal to soil moisture content (Troch *et al.*, 1999). However, because of the different source of electromagnetic radiation, the effect of vegetation on the observed signal is different to that from passive microwave observations. With active microwave remote sensing, vegetation above a soil surface absorbs and scatters part of the microwave radiation incident on it, as well as part of the reflected microwave radiation from the underneath soil surface. The amount of absorption is primarily due to the water content of the vegetation (Schmugge, 1985), whilst the scattering is influenced by the vegetation shape and geometry (van de Griend and Engman, 1985).

Various authors (van de Griend and Engman, 1985; Schmullius and Furrer, 1992; Brown *et al.*, 1992; van Zyl, 1993) have noted that the effect of vegetation on the radar signal can generally be diminished by increasing the wavelength. Schmullius and Furrer (1992) have shown that L-Band (1 to 2 GHz) measurements will still yield good results under various agricultural crops,

whereas for X- (8 to 12.5 GHz) and C-Band (4 to 8 GHz), even a thin vegetation cover may distort the measurement. It has been shown however, that C-Band data can penetrate the vegetation canopy better when the vegetation is drier (Brown *et al.*, 1992).

The effect of vegetation is also greatly dependent upon the instrument angle of incidence and polarisation (Ulaby *et al.*, 1986). Wang *et al.* (1987) have shown that the effect of vegetation cover does not play a significant role at low incidence angles.

Providing the vegetation cover is less than 15 cm, active microwave remote sensing can measure the volumetric moisture content of the near-surface soil layer with an rms error of 3.5% at low microwave frequencies (Ulaby *et al.*, 1996). However, grass covered sites often have a large volume of litter on the surface, which can hold a significant amount of water, masking the relationship between SAR data and the underlying soil moisture content (Sano *et al.*, 1998).

2.4.5.1 Optimum Satellite Configuration

Due to the sensitivity of the backscattering coefficient to surface roughness and vegetation cover, and the differing effect of various combinations of frequency and incidence angle, there has been a great deal of discussion in the literature about an “optimum” configuration for active microwave remote sensing with satellites. The recommendations that have been made in literature differ from one researcher to the next, so a brief review of the recommendations that have been made is presented below.

Soil moisture measurement using active microwave remote sensing observations is difficult due to the competing effects of soil moisture content and surface roughness. It has been noted by Chen *et al.* (1995) that the larger the incidence angle the larger the sensitivity to soil moisture content, but because of the increasing influence of surface roughness, there must be a compromise. As frequency is increased the active microwave remote sensor becomes more sensitive to surface roughness for all soil moisture conditions and sensitivity to soil moisture content decreases.

To minimise the roughness effects that may often dominate the active microwave remote sensing data in agricultural fields (eg. Koolen *et al.*, 1979; Beaudoin *et al.*, 1990), Ulaby *et al.* (1978) have suggested that the optimum parameters are frequencies from 4 to 5 GHz with *hh* polarisation having an incidence angle between 7° and 17° from nadir. This agrees closely with the recommendation made by Ulaby and Batliva (1976) who suggested that optimum parameters are a frequency of 4 GHz with *hh* or *vv* polarisation having an incidence angle between 7° and 15° from nadir, for bare fields. However, Altese *et al.* (1996) have shown that the effect of σ on backscattering is minimised by a sensor configuration having an incidence angle of around 20° and observation frequency between 4.5 and 7.5 GHz. Altese *et al.* (1996) also found that the effect of roughness correlation length l on backscattering was less than for σ , with its effect minimised at an incidence angle around 30° and observation frequency less than 6 GHz. However, Beaudoin *et al.* (1990) have shown that a significant effect on backscattering can be expected from the periodic rows of row crops at all incidence angles except around 5°, with a maximum effect in the range of 25° to 40°. In addition, Dobson and Ulaby (1986a) have suggested that the orbital sensor intended for soil moisture sensing should have an orbital inclination greater than 15° from polar orbit in order to minimise the effects of row direction at most latitudes.

Although roughness effects can be minimised by using a sensor with a low incidence angle, this configuration of look angle is very unlikely on a spacecraft system, as the resolution decreases with decreasing incidence angle according to $1/\sin\vartheta$ (Autret *et al.*, 1989). Therefore, if a low incidence angle is not acceptable, Autret *et al.* (1989) suggest that the best configuration for soil moisture measurement requires the simultaneous use of two polarisations (*hh* and *vv*) with an incidence angle greater than 35°.

To minimise the effect of vegetation on soil moisture sensing, Dobson and Ulaby (1986a) have concluded that the optimum parameters should be frequencies of less than 6 GHz and incidence angles of less than 20°. Using these observation parameters, both direct scattering by the vegetation and the effective attenuation loss related to the two-way transmission through the canopy are minimised. At

higher incidence angles, the backscattering contribution of the canopy increases and is dominated by the return from vertically aligned stalks and cobs, whereas leaves dominate the canopy loss component.

It has also been noted that the co-polarised measurements σ_{vv}^o and σ_{hh}^o , and their linear combinations, are the best choice for estimation of soil moisture content, as they are most sensitive to soil moisture changes and least sensitive to calibration accuracy and vegetation cover (Shi *et al.*, 1997). Furthermore, co-polarised channels can be calibrated directly with passive targets like corner reflectors, while cross-polarised channel calibration relies upon measurements made on the co-polarised channels (van Zyl, 1990), and is hence less accurate. Dubois *et al.* (1995a) have noted that to achieve a 4% accuracy in soil moisture content requires a 0.5 dB accuracy of the relative calibration and 2 dB accuracy in the absolute calibration.

It would therefore appear that by using ERS, which is characterised by an incidence angle of 23°, vv polarisation and frequency of 5.3 GHz (C-Band), the roughness and vegetation effects would be minimised. Thus, soil moisture inversion from ERS data for regions with short vegetation cover (plant biomass less than 1 kg m⁻²) appears more profitable than from other radar configurations (Dobson *et al.*, 1992).

Apart from satellite configuration, Schmugge (1985) has demonstrated that microwave backscattering depends more on the state of the water in the soil than on the actual amount. Thus, by expressing soil moisture as a percentage of field capacity rather than a volumetric value, Schmugge (1985) suggests that the effects of soil roughness on backscattering coefficients can be minimised.

2.4.5.2 Surface Scattering Models

The backscattering response of a surface enables important information to be determined about that surface, namely soil moisture content. Hence, much current research is being undertaken in the area for development of surface scattering models. Given the variations in satellite configuration and surface conditions, relationships between backscattering coefficient and soil moisture content as a function of incidence angle, wave polarisation, wavelength, and soil

dielectric constant are required. Three different modelling approaches have been presented in literature: (i) empirical, (ii) theoretical and (iii) semi-empirical.

The scattering coefficient, which is a unit-less quantity representing the radar cross-section (m^2) of a given pixel on the ground per unit physical area of that pixel (m^2), may exhibit a wide dynamic range, and is therefore often presented in decibels (Ulaby *et al.*, 1996). To convert the backscattering values obtained to decibels, the following relationship is used.

$$\sigma_{dB}^o = 10 \log_{10} \sigma^o \quad (2.30)$$

In the presentation of backscattering models in the following sections, the backscattering coefficient σ^o is not in decibel units, unless written as σ_{dB}^o .

2.4.5.2.1 Empirical Backscattering Models

In order to establish a useful empirical relationship for inversion of soil moisture from backscattering observations, it is necessary to have a great number of experimental measurements in order to derive general statistical laws (Oh *et al.*, 1992). However, empirical backscattering models found in literature are generally derived from specific data sets and are mostly only valid in certain regions of roughness, frequency, incidence angle and soil moisture content. Furthermore, empirical backscattering models may not be applicable for data sets other than those used in their development (Chen *et al.*, 1995; Dubois *et al.*, 1995b). Oh *et al.* (1992) have noted that the main advantage of empirical backscattering models over theoretical backscattering models is that many natural surfaces do not fall into the validity regions of the theoretical backscattering models, and even when they do, the available backscattering models fail to provide results in good agreement with experimental observations.

Much of the research to date (eg. Prevot *et al.*, 1984; Bernard *et al.*, 1986; Bruckler *et al.*, 1988; Bruckler and Witono, 1989; Ragab, 1995) has been undertaken using simple linear regression relationships between backscattering observations and observed soil moisture content in a given layer of soil.

Occasionally a second order regression equation (eg. Bruckler *et al.*, 1988) has been used. However, the form of the regression relationship commonly used is

$$\sigma_{dB}^o = a\theta + b \quad (2.31),$$

where θ is the volumetric soil moisture, and a and b are empirical regression coefficients.

Dobson and Ulaby (1986a) have found that for a given sensor combination of frequency, wave polarisation and angle of incidence, the empirically derived regression coefficients were dependent on soil surface roughness and soil texture, with a being primarily controlled by surface roughness and b primarily controlled by soil texture.

Recently, more advanced empirical non-linear regression models for relating backscattering observations to soil moisture have been presented, such as Oh's model (Oh *et al.*, 1992) and the Dubois-van Zyl model (Dubois and van Zyl, 1994; Dubois *et al.*, 1995a,b).

The empirical backscattering model of Oh *et al.* (1992) is based on L-, C- and X-Band spectrometer data, with incidence angles varying from 10° to 70°. The surface roughness and soil moisture content cover the ranges $0.1 < k_o\sigma < 6.0$, $2.6 < k_o l < 19.7$ and $0.09 < \theta < 0.31$, where k_o is the free space wave number given by $k_o = 2\pi/\lambda_o$, λ_o is the free space wavelength (cm), σ is the rms roughness height (cm), l is the roughness correlation length (cm) and θ is the volumetric soil moisture content. As backscattering from smooth surfaces include a strong contribution due to the coherent backscattering component that exists at angles close to normal incidence, the range of applicability of the backscattering model does not include the angular range below 20° for smooth surfaces. This backscattering model is presented as

$$\sigma_{vv}^o = \frac{g \cos^3 \vartheta}{\sqrt{p}} [\Gamma_v + \Gamma_h] \quad (2.32a)$$

$$\sigma_{hh}^o = g \sqrt{p} \cos^3 \vartheta [\Gamma_v + \Gamma_h] \quad (2.32b)$$

$$\sigma_{hv}^o = q \sigma_{vv}^o \quad (2.32c),$$

where

$$\sqrt{p} = 1 - \left(\frac{2\vartheta}{\pi} \right)^{\frac{1}{3\Gamma_0}} \exp(-k_o \sigma) \quad (2.33)$$

$$g = 0.7 [1 - \exp(-0.65(k_o \sigma)^{1.8})] \quad (2.34)$$

$$q = 0.23 \sqrt{\Gamma_0} [1 - \exp(-k_o \sigma)] \quad (2.35)$$

$$\Gamma_h = \frac{\left| \cos \vartheta - \sqrt{\epsilon_r - \sin^2 \vartheta} \right|^2}{\left| \cos \vartheta + \sqrt{\epsilon_r - \sin^2 \vartheta} \right|^2} \quad (2.36a)$$

$$\Gamma_v = \frac{\left| \epsilon_r \cos \vartheta - \sqrt{\epsilon_r - \sin^2 \vartheta} \right|^2}{\left| \epsilon_r \cos \vartheta + \sqrt{\epsilon_r - \sin^2 \vartheta} \right|^2} \quad (2.36b)$$

$$\Gamma_0 = \frac{\left| 1 - \sqrt{\epsilon_r} \right|^2}{\left| 1 + \sqrt{\epsilon_r} \right|^2} \quad (2.36c),$$

and ϑ is the incidence angle (degrees), Γ_v and Γ_h are the vertical and horizontal Fresnel reflectivities, Γ_0 is the Fresnel reflectivity at nadir and ϵ_r is the dielectric constant relative to free space.

The empirical backscattering model of Dubois *et al.* (1995b) was derived from two data sets, obtained from the LCX POLARSCAT and the RASAM truck-mounted systems. Equations were derived for both vv and hh polarisation and are

valid for frequencies between 1.5 and 11 GHz, surface roughness rms heights from 0.3 to 3 cm and incidence angles from 30° to 65°. This backscattering model is presented as

$$\sigma_{hh}^o = 10^{-2.75} \frac{\cos^{1.5} \vartheta}{\sin^5 \vartheta} 10^{0.028\varepsilon_r \tan \vartheta} (k_o \sigma \sin \vartheta)^{1.4} \lambda_o^{0.7} \quad (2.37a)$$

$$\sigma_{vv}^o = 10^{-2.35} \frac{\cos^3 \vartheta}{\sin^3 \vartheta} 10^{0.046\varepsilon_r \tan \vartheta} (k_o \sigma \sin \vartheta)^{1.1} \lambda_o^{0.7} \quad (2.37b),$$

where ϑ is the incidence angle (degrees), ε_r is the relative dielectric constant, k_o is the free space wave number given by $k_o = 2\pi/\lambda_o$, λ_o is the free space wavelength (cm), and σ is the rms roughness height (cm).

Omitting the usually weaker hv polarised returns was reported to make the algorithm less sensitive to system cross-talk and noise. Furthermore, co-polarised observations were reported as being less sensitive to the presence of vegetation than cross-polarised observations, thus making the algorithm more robust in the presence of vegetation than one relying on the hv polarised terms (Dubois and van Zyl, 1994; Dubois *et al.*, 1995b). However, significant amounts of vegetation were found to cause the algorithm to under-estimate soil moisture and over-estimate rms heights, as the incident electromagnetic wave failed to reach the soil surface. To address this problem, a simple criteria based on the hv cross-polarised return over the vv polarised return was developed to indicate the areas where the inversion results were more reliable, or in other words, where the vegetation was sparse enough. By masking out the areas for which the L-Band $\sigma_{hv}^o/\sigma_{vv}^o$ ratio was greater than -11 dB (corresponding to the SPOT NDVI of 0.4), reliable soil moisture estimates were obtained. Comparison with field data indicated that the algorithm could infer soil moisture content with an accuracy of 4.2% when applied to data not used in the model development (Dubois *et al.*, 1995b).

2.4.5.2.2 Theoretical Backscattering Models

Theoretical backscattering models are derived from application of the theory of electromagnetic wave scattering from a randomly rough conducting

surface (Fung *et al.*, 1992). These backscattering models are preferable to empirical and semi-empirical backscattering models, as they provide site independent relationships that are valid for different sensor configurations, and take into account the effect of different surface parameters on backscattering (Altese *et al.*, 1996). Using simplifying assumptions, theoretical backscattering models with different ranges of validity may be obtained.

The standard theoretical backscattering models are the **Kirchhoff Models (KM)**, which consists of the **Geometrical Optics Model (GOM)** and **Physical Optics Model (POM)**, and the **Small Perturbation Model (SPM)**. In a broad sense, the GOM is best suited for very rough surfaces, the POM is suited for surfaces with intermediate roughness, and the SPM is suited for surfaces with small roughness and short roughness correlation lengths (Engman and Chauhan, 1995).

In general, the like-polarised backscattering coefficients consist of a coherent (specular) term, which is important only at and near normal incidence, and a non-coherent (scattered) term, which is important at all incidence angles (Ulaby *et al.*, 1986).

For relatively rough surfaces whose backscattering coefficient exhibits a slowly varying angular dependence near nadir, the KM under the stationary phase approximation, known as the GOM, is appropriate. For such a surface the rms height σ is usually such that $k_o\sigma$ is of the order of unity. As a result, the coherent component is small in magnitude and is often much smaller than the non-coherent component. The validity conditions for the GOM are $(2k_o\sigma \cos\vartheta)^2 > 10$ and $l^2 > 2.76\sigma\lambda_o$, where k_o is the free space wave number given by $k_o = 2\pi/\lambda_o$, λ_o is the free space wavelength (cm), σ is the rms roughness height (cm), l is the roughness correlation length (cm) and ϑ is the incidence angle (degrees). Neglecting the coherent term, the GOM can be written as (Ulaby *et al.*, 1986)

$$\sigma_{pp}^o = \frac{\Gamma_o \exp\left(-\tan^2 \frac{\vartheta}{2\gamma^2}\right)}{2\gamma^2 \cos^4 \vartheta} \quad (2.38),$$

where

$$\gamma = \frac{\sigma}{l} \quad (2.39)$$

$$\Gamma_0 = \left| \frac{1 - \sqrt{\epsilon_r}}{1 + \sqrt{\epsilon_r}} \right|^2 \quad (2.40),$$

and σ_{pp}^o is the backscattering coefficient when transmission and reception are at polarisation p , Γ_0 is the Fresnel reflectivity at nadir, ϵ_r is the relative dielectric constant and γ is the surface rms slope.

The exponentially decaying angular dependence characteristic of a relatively smooth surface can be obtained using the KM under the scalar approximation, known as the POM. The validity conditions of the POM are such that $\gamma < 0.25$ and $k_o l > 6$, where γ is the surface rms slope, l is the roughness correlation length (cm), k_o is the free space wave number given by $k_o = 2\pi/\lambda_o$ and λ_o is the free space wavelength (cm). Neglecting the coherent term again, the POM may be written as (Ulaby *et al.*, 1986)

$$\begin{aligned} \sigma_{pp}^o &= 2k_o^2 \cos^2 \vartheta \Gamma_p \exp\left[-(2k_o \sigma \cos \vartheta)^2\right] \\ &\cdot \sum_{n=1}^{\infty} \left[\frac{(4k_o^2 \sigma^2 \cos^2 \vartheta)^n}{n!} \right] \\ &\cdot \int_0^{\infty} \rho^n(\xi) J_0(2k_o \xi \sin \theta) \xi d\xi \end{aligned} \quad (2.41),$$

where

$$\Gamma_h = \left| \frac{\cos \vartheta - \sqrt{\epsilon_r - \sin^2 \vartheta}}{\cos \vartheta + \sqrt{\epsilon_r - \sin^2 \vartheta}} \right|^2 \quad (2.42a)$$

$$\Gamma_v = \left| \frac{\epsilon_r \cos \vartheta - \sqrt{\epsilon_r - \sin^2 \vartheta}}{\epsilon_r \cos \vartheta + \sqrt{\epsilon_r - \sin^2 \vartheta}} \right|^2 \quad (2.42b),$$

and σ_{pp}^o is the backscattering coefficient when transmission and reception are at polarisation p , ϑ is the incidence angle (degrees), Γ_v and Γ_h are the vertical and horizontal Fresnel reflectivities, ϵ_r is the relative dielectric constant, σ is the rms roughness height (cm), $\rho(\xi)$ is the single parameter surface correlation function and $J_0(\)$ is the zeroth order Bessel function of the first kind. In computing (2.41), the error incurred in truncating the summation at $n = 10$ is less than 0.1 dB (Ulaby *et al.*, 1986).

The SPM given by (2.43) has the validity conditions of $\gamma < 0.3$ and $k_o\sigma < 0.3$, where γ is the rms surface slope, k_o is the free space wave number given by $k_o = 2\pi/\lambda_o$, λ_o is the free space wavelength (cm) and σ is the rms roughness height (cm) (Ulaby *et al.*, 1986).

$$\sigma_{pq}^o = 8|\alpha_{pq}|^2 k_o^4 \sigma^2 \cos^4 \vartheta W(2k_o \sin \vartheta) \quad (2.43),$$

where

$$\alpha_{hh} = \frac{\cos \vartheta - \sqrt{\epsilon_r - \sin^2 \vartheta}}{\cos \vartheta + \sqrt{\epsilon_r - \sin^2 \vartheta}} \quad (2.44a)$$

$$\alpha_{vv} = (\epsilon_r - 1) \frac{\sin^2 \vartheta - \epsilon_r (1 + \sin^2 \vartheta)}{\left[\epsilon_r \cos \vartheta + \sqrt{\epsilon_r - \sin^2 \vartheta} \right]^2} \quad (2.44b),$$

and σ_{pq}^o is the backscattering coefficient when transmission is at polarisation p and reception is at polarisation q , ϑ is the incidence angle (degrees) and ϵ_r is the relative dielectric constant. $W(\)$ is the normalised roughness spectrum, which is the Bessel transform of the single parameter correlation function $\rho(\xi)$, evaluated at the surface wave number of $2k_o \sin \vartheta$. For the Gaussian correlation function $\rho(\xi) = \exp(-\xi^2/l^2)$, the normalised roughness spectrum is given by

$$W(2k_o \sin \vartheta) = \frac{1}{2} l^2 \exp\left[-(k_o l \sin \vartheta)^2\right] \quad (2.45).$$

The **Integral Equation Model (IEM)** was developed by Fung *et al.* (1992), and is shown to unite the KM and SPM, hence making it applicable to a wider range of roughness conditions or frequencies. In its complete version, the model describes the backscattering behaviour of a random rough bare surface without any limitation on the roughness scale or frequency range, and accounts for both single and multiple surface scattering of a conducting surface. Because of its complexity, it is not practical to use the complete version of the IEM and in applications approximate solutions are usually considered.

Altese *et al.* (1996) have used an approximate version of the IEM, which is valid for surfaces with small to moderate surface rms heights (Fung *et al.*, 1992). The validity expression for this model may be expressed as $k_o\sigma < 3$, where $k_o = 2\pi/\lambda_o$ is the free space wave number, λ_o is the free space wavelength (cm) and σ is the rms roughness height (cm). Altese *et al.* (1996) used only the single scattering component of the IEM and made further simplifying assumptions by using only the real part of the relative dielectric constant and assuming that the surface correlation function is isotropic and can be represented by either the Gaussian or exponential models.

As most natural terrains have a small rms surface slope, it has been suggested by Fung *et al.* (1992) that single scattering terms should dominate over multiple scattering terms in most situations. The conditions under which significant multiple scattering has been found to occur are: (i) normalised surface height $k_o\sigma > 1$; and (ii) surface rms slope $\gamma > 0.5$ (Hsieh and Fung, 1997).

The approximate version of the IEM used by Altese *et al.* (1996) is presented in (2.46), with p and q representing either h or v polarisation. This algorithm has been used successfully by Su *et al.* (1997) to estimate volumetric soil moisture content in bare fields during the **European Multi-sensor Airborne Campaign 1994 (EMAC'94)**.

$$\sigma_{pq}^o = \frac{k_o^2}{2} \exp(-2k_{zo}^2 \sigma^2) \sum_{n=1}^{\infty} \sigma^{2n} |I_{pq}^n|^2 \frac{W^n(-2k_{xo}, 0)}{n!} \quad (2.46),$$

where

$$I_{pq}^n = (2k_{zo})^n f_{pq} \exp(-\sigma^2 k_{zo}^2) + \frac{k_{zo}^n [F_{pq}(-k_{xo}, 0) + F_{pq}(k_{xo}, 0)]}{2} \quad (2.47)$$

$$f_{vv} = \frac{2R_v}{\cos \vartheta} \quad (2.48a)$$

$$f_{hh} = \frac{-2R_h}{\cos \vartheta} \quad (2.48b)$$

$$F_{vv}(-k_{xo}, 0) + F_{vv}(k_{xo}, 0) = \frac{2 \sin^2 \vartheta (1 + R_v)^2}{\cos \vartheta} \cdot \left[\left(1 - \frac{1}{\epsilon_r} \right) + \frac{\mu_r \epsilon_r - \sin^2 \vartheta - \epsilon_r \cos^2 \vartheta}{\epsilon_r^2 \cos^2 \vartheta} \right] \quad (2.49a)$$

$$F_{hh}(-k_{xo}, 0) + F_{hh}(k_{xo}, 0) = \frac{-2 \sin^2 \vartheta (1 + R_h)^2}{\cos \vartheta} \cdot \left[\left(1 - \frac{1}{\mu_r} \right) + \frac{\mu_r \epsilon_r - \sin^2 \vartheta - \mu_r \cos^2 \vartheta}{\mu_r^2 \cos^2 \vartheta} \right] \quad (2.49b)$$

$$R_h = \frac{\cos \vartheta - \sqrt{\epsilon_r - \sin^2 \vartheta}}{\cos \vartheta + \sqrt{\epsilon_r - \sin^2 \vartheta}} \quad (2.50a)$$

$$R_v = \frac{\epsilon_r \cos \vartheta - \sqrt{\epsilon_r - \sin^2 \vartheta}}{\epsilon_r \cos \vartheta + \sqrt{\epsilon_r - \sin^2 \vartheta}} \quad (2.50b)$$

$$R_0 = \frac{1 - \sqrt{\epsilon_r}}{1 + \sqrt{\epsilon_r}} \quad (2.50c)$$

$$W^n(u, v) = \frac{1}{2\pi} \int_{-\infty}^{+\infty} \rho^n(\xi, \zeta) \exp(-iu\xi - iv\zeta) d\xi d\zeta \quad (2.51),$$

and f_{pq} is the Kirchhoff coefficient, F_{pq} is the complementary field coefficient, R_v and R_h are the vertical and horizontal Fresnel reflection coefficients, R_0 is the Fresnel reflection coefficient at nadir, ϵ_r is the relative dielectric constant, k_o is the free space wave number given by $k_o = 2\pi/\lambda_o$, λ_o is the free space wavelength (cm), k_{zo} is the z component of the free space wave number given by $k_{zo} = k_o \cos\vartheta$, k_{xo} is the x component of the free space wave number given by $k_{xo} = k_o \sin\vartheta$, σ is the rms surface height (cm), l is the correlation length (cm) and μ_r is the relative magnetic permeability, which is usually equal to unity for soil, since soil rarely contains significant amounts of ferromagnetic components (Roth *et al.*, 1990).

W^n is the roughness spectrum of the surface related to the n th power of the two parameter surface correlation function $\rho(\xi, \zeta)$ by the Fourier transformation, and is usually simplified to a single parameter isotropic case (Fung, 1994). The Fourier transform of the n th power of the: (i) Gaussian correlation function is given in (2.52a); (ii) exponential correlation function is given in (2.52b); and (iii) 1.5 power correlation function is given in (2.52c).

$$W^n(K) = \frac{l^2}{2n} \exp\left[\frac{-(Kl)^2}{4n}\right] \quad (2.52a)$$

$$W^n(K) = \left(\frac{l}{n}\right)^2 \left[1 + \left(\frac{Kl}{n}\right)^2\right]^{-1.5} \quad (2.52b)$$

$$W^n(K) = \frac{l^2 K^{1.5n-1} J_{-(1.5n-1)}(K)}{2^{1.5n-1} \Gamma(1.5n)} \quad (2.52c),$$

where l is the roughness correlation length (cm), $\Gamma(\)$ is the gamma function, and $J_\nu(\)$ is the Bessel function of the second kind of order ν with the imaginary argument.

Fung (1994) notes that for dielectric surfaces there are two approximations that have been made to the local angle in the Fresnel reflection coefficients R_v and R_h to be used in the Kirchhoff coefficient f_{pq} . One approximation replaces the local angle by the incident angle and the other by the angle along the specular direction. The local angle in the Fresnel reflection coefficients in the complementary field coefficients F_{qp} is always approximated by the incident angle. Fung (1994) has shown that the approximation by the incident angle is good for the low to intermediate frequency region while the other approximation is good in the high frequency region. Thus, it has been proposed by Fung (1994) that for $k_o \sigma k_o l < a \sqrt{\epsilon_p}$, ϑ is the incident angle, and for $k_o \sigma k_o l > a \sqrt{\epsilon_p}$, ϑ is equal to 0° , where a is 1.2, 1.6 and 200 for Gaussian, 1.5 power, and exponential surface roughness correlation functions respectively.

An alternative method for estimating the incidence angle in the reflection coefficients used in the Kirchhoff coefficient has been proposed by Wu *et al.* (1997), which uses a transition function to go between R_ϑ and R_0 in the intermediate frequency region. The reflection coefficient used is given by

$$R_T = R_\vartheta + [R_0 - R_\vartheta] T^2 \quad (2.53),$$

where

$$T = 1 + \pi^{-1} \left\{ \tan^{-1} \left[2.5 \gamma \sigma^2 \cos^2 \vartheta (k_o^2 - 1.3 k_{\sigma r}^2) \right] - 0.5 \pi \right\} \quad (2.54),$$

and γ is the rms surface slope given by σ/l , σ is rms surface roughness (cm), l is the correlation length (cm), R_0 is the reflection coefficient at nadir, R_ϑ is the reflection coefficient at the incidence angle, and $k_{\sigma r}$ is the free space wave number at transition frequency f_r . It is suggested by Wu *et al.* (1997) that the transition frequency used is the maximum frequency corresponding to the cross point between IEM and GOM. In the case where there is no cross point, then it is suggested that the transition frequency be set to the frequency corresponding to the peak value of backscattering from the IEM with R_ϑ .

Theoretical models can predict reasonably well the general trend of backscattering coefficient in response to changes in roughness or soil moisture content. However, because of their complexity or the restrictive assumptions made when deriving them, it has been reported by various researchers (Oh *et al.*, 1992; Dubois and van Zyl, 1994; Dubois *et al.*, 1995b) that they can rarely be used to invert data measured from natural surfaces, due to failure of satisfying validity regions or in providing results in good agreement with experimental observations.

Chen and Fung (1995) have examined the ease of applicability and accuracy of three theoretical surface scattering models when compared with exact moment method simulations. The models examined were the IEM, the **F**ull **W**ave **M**odel (FWM) and the **P**hase **P**erturbation **M**odel (PPM). The most complex of these is the FWM, which requires evaluation of a ten-fold integral (reduces to two double integrals under certain assumptions), and the simplest is the IEM. This study found only the IEM and PPM to accurately predict the backscattering coefficient over all incident angles, with the IEM being the fastest to evaluate, and the PPM being significantly slower.

2.4.5.2.3 *Semi-Empirical Backscattering Models*

Semi-empirical backscattering models are an improvement to empirical backscattering models in so much as they either start from a theoretical background and then use simulated or experimental data sets to simplify the theoretical backscattering model. Alternatively, they use simulated data from a theoretical backscattering model to derive an empirical backscattering model that describes the backscattering response for a wide range of surface conditions. The main advantage of these backscattering models is that they are not expected to have the site-specific problems commonly associated with empirical backscattering models derived from a limited number of observations.

Among the first semi-empirical backscattering models is that of Oh *et al.* (1994). This model is based on existing theoretical backscattering models (SPM and KM) in conjunction with extensive experimental data, and is an extension of their previously developed empirical model (2.32), to include both the magnitude

and phase of the backscattering. The experimental data that was used to solve for the unknown constants of the expression chosen to represent the backscattering response of a surface, was collected from a truck-mounted L-, C- and X-Band polarimetric scatterometer over a range of incidence angles from 10° to 70°. The expression chosen for the vv polarised backscattering was

$$\sigma_{vv}^o = 13.5 \exp\left(-1.4(k_o \sigma)^{0.2}\right) \frac{1}{\sqrt{p}} \Gamma_h (k_o \sigma)^2 (\cos \vartheta)^{3.25-0.05k_o l} \exp\left(-(2k_o \sigma \cos \vartheta)^{0.6}\right) W \quad (2.55),$$

where

$$\sqrt{p} = 1 - \left(\frac{2\vartheta}{\pi}\right)^{\Gamma_0} \exp(-k_o \sigma) \quad (2.56)$$

$$W = \frac{(k_o l)^2}{1 + (2.6k_o l \sin \vartheta)^2} \left[1 - 0.71 \frac{1 - 3(2.6k_o l \sin \vartheta)^2}{[1 + (2.6k_o l \sin \vartheta)^2]^2} \right] \quad (2.57),$$

and k_o is the free space wave number given by $k_o = 2\pi/\lambda_o$, λ_o is the free space wavelength (cm), σ is the rms roughness height (cm), l is the roughness correlation length (cm), ϑ is the incidence angle (degrees), Γ_h is the horizontal Fresnel reflectivity given by (2.36a) and Γ_0 is the Fresnel reflectivity at nadir given by (2.36c). W is the roughness spectrum corresponding to a quadratic exponential correlation function, which was found by Oh *et al.* (1994) to be the form of the correlation function that best describes the roughness of natural fields.

Chen *et al.* (1995) have also developed a semi-empirical backscattering model, which is based on the single scattering terms of the IEM. It is a multiple linear regression model of simulated data using the IEM with the assumption that surface roughness can be described by an exponential correlation function. The ratio of vv and hh backscattering coefficients were used to describe the backscattering response of the surface, as simulations of backscattering coefficient were found to be less sensitive to the effects of both surface roughness and

incidence angle uncertainty using this ratio. The data generated in the simulation procedure had the following ranges: volumetric soil moisture 10 to 40% v/v, roughness correlation length 1 to 15 cm, rms roughness height 0.1 to 2 cm, incidence angle 10° to 50° and observation frequency 1 to 10 GHz. The final form of the linear regression equation developed is given by

$$\ln \theta = -0.09544 \sigma_{hh/vv_{dB}}^o - 0.00971 \vartheta + 0.029238 \times 10^{-9} f - 1.74678 \quad (2.58),$$

where θ is the volumetric soil moisture fraction, $\sigma_{hh/vv_{dB}}^o$ is the ratio of hh to vv polarisation backscattering in dB, ϑ is the incidence angle in degrees and f is the observation frequency in Hz.

Another semi-empirical backscattering model is that of Shi *et al.* (1997), which is also based on the single scattering terms of the IEM. The development of this model relied on non-linear fitting of IEM based numerical simulations for a wide range of surface roughness and soil moisture conditions at very fine intervals. The algorithm was then applied to AIRSAR (aircraft) and SIR-C (space shuttle) measurements over bare and sparse short vegetated surfaces for inferring soil moisture content and surface roughness. As with the model of Chen *et al.* (1995), no measured data were used in the algorithm development. The equations derived are for surfaces with rms heights from 0.2 to 3.6 cm, roughness correlation lengths ranging from 2.5 to 35 cm, incidence angles between 25° and 70° and moisture contents from 2 to 50% v/v. All calibration and evaluation was undertaken with measurements at L-Band (1.25 GHz), and a power correlation function with exponent $n = 1, 1.2$ and 1.4 .

The base model used by Shi *et al.* (1997) is

$$\sigma_{pq}^o = |\alpha_{pq}|^2 \left[\frac{S_R}{a_{pq}(\vartheta) + b_{pq}(\vartheta) S_R} \right] \quad (2.59),$$

where

$$S_R = (k_o \sigma)^2 W(-2k_{x_o}) \quad (2.60)$$

$$W(K) = \int_0^\infty \rho(\xi) J_0(K\xi) \xi d\xi \quad (2.61)$$

$$\alpha_{vv} = 4k_o \left[R_v \cos^2 \vartheta + \frac{\sin^2 \vartheta (1 + R_v)^2}{2} \left(1 - \frac{1}{\epsilon_r} \right) \right] \quad (2.62a)$$

$$\alpha_{hh} = -4k_o R_h \cos^2 \vartheta \quad (2.62b)$$

$$a_{vv}(\vartheta) = \exp(-3.118 + 5.302\vartheta) \quad (2.63a)$$

$$b_{vv}(\vartheta) = \exp(-3.013 + 2.361 \tan^{6.8} \vartheta) \quad (2.63b)$$

$$R_h = \frac{\cos \vartheta - \sqrt{\epsilon_r - \sin^2 \vartheta}}{\cos \vartheta + \sqrt{\epsilon_r - \sin^2 \vartheta}} \quad (2.64a)$$

$$R_v = \frac{\epsilon_r \cos \vartheta - \sqrt{\epsilon_r - \sin^2 \vartheta}}{\epsilon_r \cos \vartheta + \sqrt{\epsilon_r - \sin^2 \vartheta}} \quad (2.64b),$$

and σ_{pq}^o is the backscattering coefficient when transmission is at polarisation p and reception is at polarisation q ; S_R is a roughness parameter that accounts for rms roughness height σ (cm), correlation length l (cm) and correlation function; W is the roughness spectrum related to a one-parameter surface correlation function $\rho(\xi)$; $J_0(\)$ is the Bessel function to zeroth order; k_o is the free space wave number given by $k_o = 2\pi/\lambda_o$, λ_o is the free space wavelength (cm) and k_{x_o} is the x component of the free space wave number given by $k_{x_o} = k_o \cos \vartheta$; ϑ is the incidence angle (degrees); a_{pq} and b_{pq} are empirically derived coefficients; α_{pq} is an approximation to the parameter I_{pq} in the IEM, which holds for $k_o \sigma \ll 1$; R_v and R_h

are the vertical and horizontal Fresnel reflection coefficients; and ϵ_r is the relative dielectric constant.

By using two polarisation measurements and rearranging the above equations, Shi *et al.* (1997) eliminated the roughness parameter S_r to obtain

$$10 \log_{10} \left[\frac{|\alpha_{vv}|^2 + |\alpha_{hh}|^2}{\sigma_{vv}^o + \sigma_{hh}^o} \right] = a_{vh}(\vartheta) + b_{vh}(\vartheta) 10 \log_{10} \left[\frac{|\alpha_{vv}| |\alpha_{hh}|}{\sqrt{\sigma_{vv}^o \sigma_{hh}^o}} \right] \quad (2.65),$$

where

$$a_{vh}(\vartheta) = \exp \left(\frac{-12.37 + 37.206 \sin \vartheta - 41.187 \sin^2 \vartheta + 18.89 \sin^3 \vartheta}{41.187 \sin^2 \vartheta + 18.89 \sin^3 \vartheta} \right) \quad (2.66a)$$

$$b_{vh}(\vartheta) = 0.649 + 0.659 \cos \vartheta - 0.306 \cos^2 \vartheta \quad (2.66b).$$

Shi *et al.* (1997) used (2.65) to solve for the dielectric constant of the near-surface soil layer from *vv* and *hh* polarisation observations, and then used (2.59) to solve for the surface roughness parameter.

2.4.5.3 Volume Scattering Model

If the dielectric properties of the soil are homogeneous with depth, backscattering of the electromagnetic wave occurs solely at the soil surface, and is known as surface scattering. However, if a soil moisture (dielectric) gradient exists near the soil surface, the dielectric properties of the soil are inhomogeneous, and part of the transmitted wave is also backscattered due to scattering within the volume of the soil medium, known as volume scattering. This volume scattering is the result of electromagnetic radiation entering the soil and then being backscattered from a dielectric discontinuity in the soil medium (Ulaby *et al.*, 1982), as illustrated in Figure 2.19.

All of the backscattering models described in the previous section neglect these gradients, and estimate only the surface scattering term as a function of the

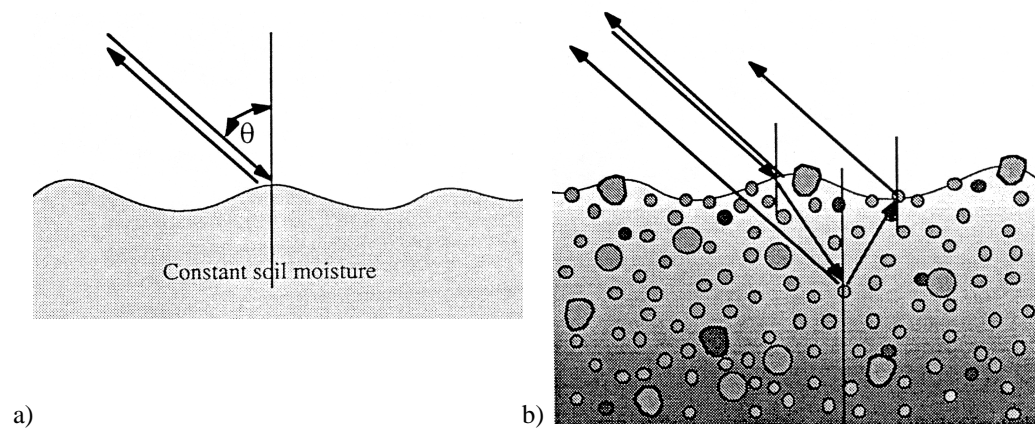


Figure 2.19: Illustration of a) surface scattering as modelled by the standard IEM, and b) surface and volume scattering as modelled by the modified IEM (Fung *et al.*, 1996).

dielectric constant at the air-soil interface. The justification for this has been that the discontinuity in dielectric constant at the air-soil interface has the greatest effect on backscattering for natural profiles, since such profiles do not usually exhibit sharp discontinuities within the soil medium. However, small variations in the shape of the dielectric profile can still result in significant changes in the total backscattering coefficient (Ulaby *et al.*, 1978).

To account for the varying dielectric profile in the existing surface scattering models, an equivalent soil moisture value over a fixed depth is assumed (Boisvert *et al.*, 1997). Several approaches have been presented in the literature for determining this equivalent soil moisture value, and are outlined in Ulaby and Batliva (1976). The approaches include: (i) the fixed depth soil moisture content, which is the average moisture content in a near-surface soil layer; (ii) the equivalent skin depth soil moisture content, which is the soil moisture content of a homogeneous medium whose skin depth at the frequency of interest is identical to the skin depth of the soil medium under investigation; (iii) the equivalent coherent reflection soil moisture content; and (iv) the equivalent incoherent soil moisture content. Boisvert *et al.* (1997) have shown that a mean fixed depth was sufficient to relate σ' to the dielectric constant when there was no soil moisture gradient, but overestimated σ' in the presence of a gradient.

Whilst using an equivalent soil moisture content in the existing surface scattering models has attempted to account for the soil moisture gradients that are common place in the natural environment, it has not accounted for the

backscattering contribution from the soil volume. To account for the effects of volume scattering, Fung *et al.* (1996) have proposed a Modified IEM, which incorporates a physical dielectric gradient into the backscattering model. The effect of a vertical dielectric profile was incorporated by replacing the standard Fresnel reflection coefficients with the modified set of reflection coefficients

$$R_h = \frac{\Gamma(is \cos \vartheta)}{\Gamma(-is \cos \vartheta)} \frac{\Gamma\left[\left(\frac{-is}{2}\right)\left(\cos \vartheta + \sqrt{\cos^2 \vartheta + (\epsilon_{r_\infty} - 1)}\right)\right]}{\Gamma\left[\left(\frac{is}{2}\right)\left(\cos \vartheta - \sqrt{\cos^2 \vartheta + (\epsilon_{r_\infty} - 1)}\right)\right]} \quad (2.67a)$$

$$\cdot \frac{\Gamma\left[1 - \left(\frac{is}{2}\right)\left(\cos \vartheta + \sqrt{\cos^2 \vartheta + (\epsilon_{r_\infty} - 1)}\right)\right]}{\Gamma\left[1 + \left(\frac{is}{2}\right)\left(\cos \vartheta - \sqrt{\cos^2 \vartheta + (\epsilon_{r_\infty} - 1)}\right)\right]}$$

$$R_v = \frac{\Gamma(is \cos \theta)}{\Gamma(-is \cos \theta)} \frac{\Gamma\left[\left(\frac{-is}{2}\right)\left(\cos \vartheta + \frac{1}{\epsilon_{r_\infty}} \sqrt{\cos^2 \vartheta + (\epsilon_{r_\infty} - 1)}\right)\right]}{\Gamma\left[\left(\frac{is}{2}\right)\left(\cos \vartheta - \frac{1}{\epsilon_{r_\infty}} \sqrt{\cos^2 \vartheta + (\epsilon_{r_\infty} - 1)}\right)\right]} \quad (2.67b),$$

$$\cdot \frac{\Gamma\left[1 - \left(\frac{is}{2}\right)\left(\epsilon_{r_\infty}^{\frac{1}{3}} \cos \vartheta + \sqrt{\cos^2 \vartheta + (\epsilon_{r_\infty} - 1)}\right)\right]}{\Gamma\left[1 + \left(\frac{is}{2}\right)\left(\cos \vartheta - \sqrt{\cos^2 \vartheta + (\epsilon_{r_\infty} - 1)}\right)\right]}$$

where $\Gamma(\cdot)$ is the gamma function, ϑ is the incidence angle (degrees), $s = 2k_o/m$, k_o is the free space wave number given by $k_o = 2\pi/\lambda_o$, λ_o is the free space wavelength (cm) and m is the transition rate factor (cm^{-1}) explained below.

In the formulation of the modified reflection coefficients to account for a drying profile, the transitional dielectric layer was modelled by an exponential dielectric profile in which the dielectric constant as a function of depth z (cm) is

$$\epsilon_r(z) = 1 + (\epsilon_{r_\infty} - 1) \frac{\exp(mz)}{1 + \exp(mz)} \quad (2.68).$$

The inputs to this dielectric model are the transition rate factor m and the dielectric constant at depth $z = \infty$ ($\epsilon_{r_{\infty}}$). By (2.68) the relative dielectric constant $\epsilon_r(z)$ starts from 1 in air and gradually changes to $\epsilon_{r_{\infty}}$ at the rate m . Fung *et al.* (1996) have suggested that a value for m equal to about 12 cm^{-1} should be appropriate, and was shown to give an improvement in the simulation of backscattering when compared to the standard IEM.

2.4.5.4 Evaluation of Surface Scattering Models

Hoeben *et al.* (1999) have undertaken an evaluation of surface scattering models for the smooth and very rough surface data sets measured in the **E**uropean **M**icrowave **S**ignature **L**aboratory (EMSL) experiment (Mancini *et al.*, 1995; discussed in Chapter 4). In this evaluation, only the vv and hh co-polarisation responses were simulated, using the empirical models of Oh (2.32) and Dubois-van Zyl (2.37), and the approximate version of the theoretical IEM (2.46). Simulations were made using the measurement of the real part of the dielectric constant at a depth of 2.5 cm, and compared with the measured backscattering response.

The results of this evaluation indicated that for the smooth surface, the IEM was the only model that performed well. However, for the rough surface under drying conditions, all three models gave reasonable results. It was also indicated that care should be taken with measurements of smooth surfaces at incidence angles approaching 35° , as there was some doubt as to whether the model incorrectly predicted the backscattering or if there was noise in the measurements. It was also suggested that simplification of the IEM has resulted in a significant loss in accuracy.

A study by Mancini *et al.* (1996), which also evaluates the IEM with EMSL data, suggests that the IEM predicts the trend for σ^o well for forward modelling over the whole range of frequencies, despite the fact that the observed backscattering showed oscillations with frequency (Figure 2.20). However, when applying the inversion mode, the computed surface dielectric constant was found reliably for the smooth surface, but for the rough surface, the combined effect of

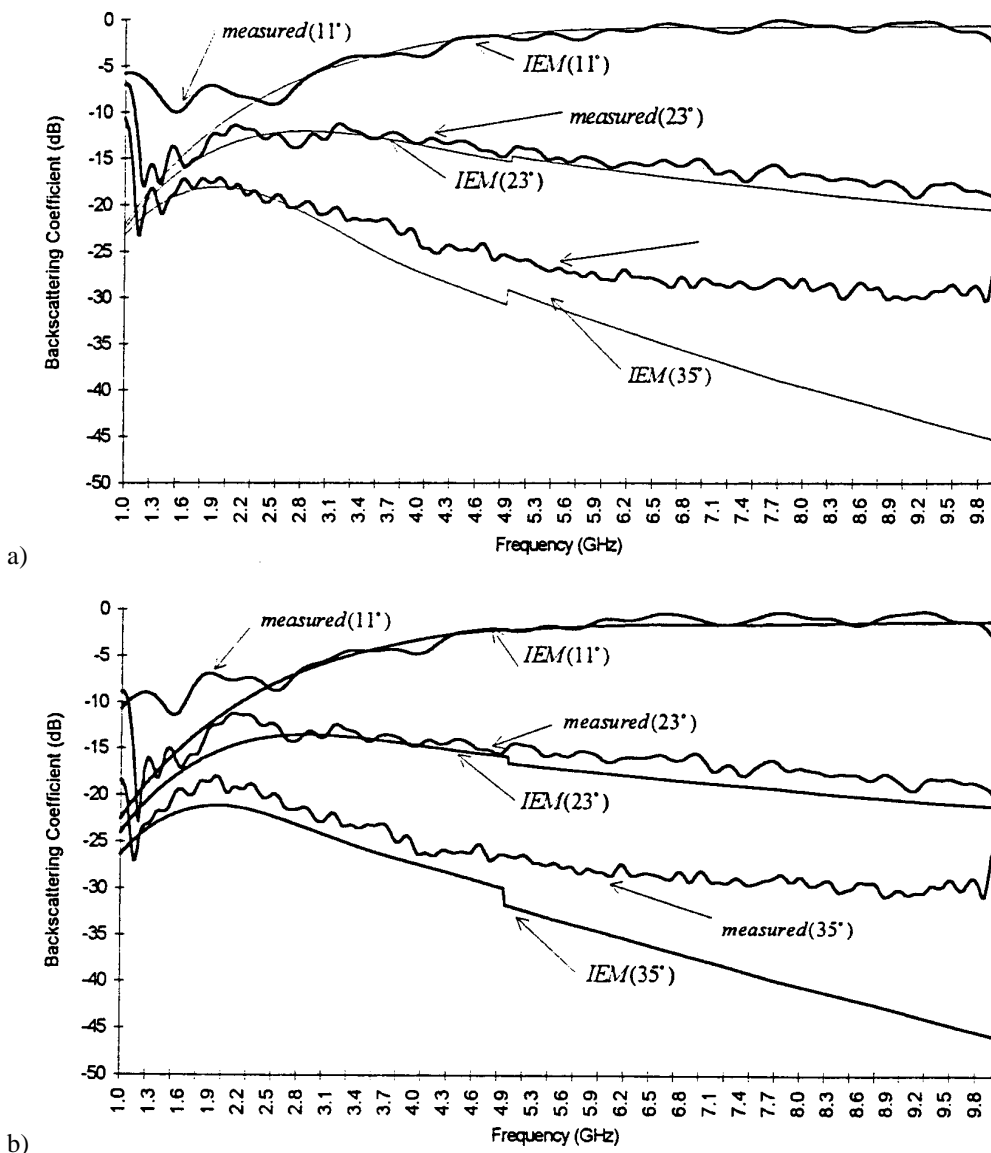


Figure 2.20: Comparison of IEM estimate of backscattering coefficient with the observed backscattering coefficient from the smooth EMSL experiment at incidence angles of 11°, 23° and 35° (Mancini *et al.*, 1996).

relatively high dielectric constant and the oscillations in the measured backscattering produced large fluctuations in the retrieved dielectric constant.

2.4.5.5 Surface Roughness Effects

Surface roughness characteristics have generally been described in terms of the rms surface height σ , roughness correlation length l , and a correlation function. Altese *et al.* (1996) have shown that the behaviour of the IEM is highly dependent on the choice of the correlation function. Furthermore, it has been

shown by Wegmüller *et al.* (1994) that the exponential correlation function usually gives a better agreement to the observed correlation function than the Gaussian correlation function in agricultural fields. Of the roughness parameters, Jackson *et al.* (1997) suggests that rms surface height is the most important.

The method used to evaluate the roughness parameters has generally involved physically measuring the horizontal surface profile for a 1 to 2 m length at various locations over the site, using one of four methods. These methods have included: (i) inserting a thin metal plate vertically into the soil and then spraying with paint from an approximately horizontal direction; (ii) taking a photograph of the intersection of the ground surface with a gridded plate and digitising the intersection; (iii) using a panel with drop pins, and (iv) using a laser profiler (Ulaby and Batliva, 1976; Ulaby *et al.*, 1978; Troch *et al.*, 1994; Wegmüller *et al.*, 1994). These profiles are generally taken in several directions for each location (Troch *et al.*, 1994). As there is no rule for choosing the spacing of roughness measurements along the profile, the suggestion of Ulaby *et al.* (1986) is often followed, using a spacing approximately equal to one-tenth of the free space wavelength.

Lin (1994) and Wang *et al.* (1997) have noted that the commonly used sampling techniques for measuring field surface roughness parameters required in microwave backscattering models are questionable, especially for smooth fields. This is because they have measurement scales of the order of a few metres, which is significantly smaller than the application scale when inferring near-surface soil moisture content from remote sensing observations. Moreover, it is questionable whether the correlation length can be adequately estimated from surface profiles of this length (Wang *et al.*, 1987). Oh (1997) showed that to estimate the surface roughness parameters with a precision of $\pm 5\%$, the surface must be sampled at a spacing of less than $0.2l$ and that the segment length be at least $200l$, where l is the correlation length.

From the study of Altese *et al.* (1996), it is clear that soil roughness characteristics are very important for determining the surface backscattering properties of fields. Their study concludes that for very smooth surfaces ($\sigma < 1$ cm), it is impossible to use SAR soil moisture inversion algorithms because

of the sensitivity of σ' with respect to σ . However, as the surface becomes rougher ($\sigma > 1$ cm) the sensitivity to roughness decreases (Altese *et al.*, 1996; Sano *et al.*, 1998). Hence, as regular agricultural fields generally have $\sigma > 1$ cm, this problem should not be relevant for routine use (Altese *et al.*, 1996). It should also be noted that roughness parameters are not constant, at least for bare fields, with heavy rain causing erosion and smoothing of the soil surface (Wegmüller *et al.*, 1994).

To overcome the surface roughness problem, Jackson *et al.* (1997) suggested a procedure for developing a global roughness data set as a first order correction in soil moisture inversion algorithms, based on land cover and use. For agricultural fields, Jackson *et al.* (1997) suggest a roughness value of 1.5 cm as being the most representative, which should be reduced by a rainfall reduction factor, $0.89\exp(-0.026P)$, where P is the cumulative precipitation (cm) since tillage. Unlike agricultural areas, the roughness height of rangeland and grassland is more or less constant over time. It is further suggested by Jackson *et al.* (1997) that land use be grouped into the land cover types of sod grass, bunch grass and shrub/brush with roughness heights of 0.8, 1.4 and 1.8 cm.

Since there is no immediate hope of developing a surface roughness measurement technique with a measurement scale comparable to the application scale, and since it is too complex to develop a theory to bridge the gap between measurement and application scales, Lin (1994) and Wütherich (1997) suggest an alternative data analysis scheme that uses field roughness measurements as a quality control measure only. This scheme involves collecting near-surface soil moisture content data by TDR on a grid, and then solving for surface roughness using a microwave backscattering model. Comparison of the roughness characteristics evaluated can then be made with the field collected roughness data. However, a small error in soil moisture content results in a large error in surface roughness, and using such to invert soil moisture again carries large uncertainties (Wütherich, 1997). Altese *et al.* (1996) have found that for σ less than 1 cm, an error of 0.01 cm in the measurement of rms height can imply an error in the inferred soil moisture content of up to 8% v/v, while for σ greater than 1 cm, an error of 0.01 cm in the measurement of rms surface height can imply an error in the retrieved soil moisture content of only about 0.3% v/v.

Due to the high level of field work required to determine roughness parameters using the above methods, and the fact that roughness parameters cannot be measured with the required degree of accuracy (Wütherich, 1997), Su *et al.* (1995, 1997) have proposed an alternative solution. The method is to simultaneously infer both surface roughness parameters and soil moisture content, using multiple remote sensing measurements at different wavelengths or polarisations.

Due to the sensitivity of backscattering to surface roughness parameters (Altese *et al.*, 1996; Lin, 1994; Su *et al.*, 1995, 1997), Su and Troch (1996) undertook a study to fully determine the relationship between radar backscattering and soil surface parameters under different antenna configurations. This study showed that as the soil becomes wetter the sensitivity of σ^o to ϵ_r decreases, with a 5 dB change in σ^o due to a change in ϵ_r from 5 to 25 (10 to 40% volumetric soil moisture), independent of radar configuration and surface roughness conditions. Su and Troch (1996) were able to show that an accuracy of 0.1 cm and 1 cm in determining σ and l respectively can be considered satisfactory for determining σ^o regardless of soil moisture content, given that the roughness conditions for most agricultural fields generally lie within 0.5 to 2.0 cm in σ and from 5 to 20 cm in l . The study also concluded that low frequencies and low incidence angle configurations are more favourable for inferring soil moisture content, with the sensitivity of σ^o to changes in σ and l decreasing.

Following on from the study by Su and Troch (1996), Hoeben *et al.* (1997) have shown that an accurate knowledge about the correlation length is important at lower incidence angles, while the rms surface roughness has to be accurately known at higher incidence angles.

2.4.5.6 Vegetation Effects

In the presence of a vegetation canopy, there is a combination of volume scattering and attenuation by the vegetation layer, and surface scattering by the underlying soil surface. The relative importance of these two contributions is dependent on several factors, including the vegetation penetration depth, the canopy height, observation frequency, wave polarisation and the angle of

incidence. The effect of a significantly vegetated surface, is to increase the backscatter compared to a bare surface, with the effect being relatively large for the cross-polarised channel. The degree to which vegetation affects the determination of soil moisture content depends on several factors: vegetation biomass, canopy type and configuration, and crop condition (Schmugge *et al.*, 1980; D’Urso *et al.*, 1994). In addition, Dobson and Ulaby (1986a) have shown that at low soil moisture contents, the backscattering contributions from the crop canopy itself dominate the total return.

The penetration depth in vegetation is difficult to estimate, due to the difficulty in establishing the effective dielectric constant of the vegetated medium. Indirect estimates, obtained by comparing backscattering coefficient close to nadir for bare soil and vegetated soil, have indicated that the penetration depth of mature crops in the green stage is typically several metres at frequencies around 1 GHz, and decreases to one metre or less at frequencies above 10 GHz (Ulaby *et al.*, 1982). The main factors that influence the penetration depth are the geometry of the canopy and the vegetation biomass of the canopy. If the plant moisture content is low, the penetration depth can be higher than if the vegetation is moist and lush, as the absorption by the vegetation is primarily due to the water content in the vegetation. It has also been noted that the attenuation for horizontal polarisation is very weak, but the vertically polarised data are attenuated to a much greater degree because of the relationship with the canopy structure, which consists primarily of vertical stalks (Engman and Chauhan, 1995).

In order to determine soil moisture content of heavily vegetated terrain, the effects of the vegetation canopy must be determined. The quantitative estimation of near-surface soil moisture content under a vegetation layer has historically been obtained from an empirical relationship of the form given in (2.31) (eg. Dobson and Ulaby, 1986b; Wood *et al.*, 1993). However, these empirical relationships are site specific and therefore have limited ranges of validity. Thus, the development of theoretical models that account for vegetated terrains are useful for studying the dominant factors controlling the backscattering process (Engman and Chauhan, 1995; Troch *et al.*, 1999). The theoretical backscattering models that account for vegetation generally require a large number of parameters to be measured or estimated in the field. For example, the backscattering model used by Lin *et al.*

(1994b) requires more than 20 parameters, including; frequency, local incidence angle, length of the semi-minor and semi-major axes of the leaves, leaf thickness, type and parameter of leaf orientational distribution, density of leaves, leaf dielectric constant, length and radius of stem, type and parameter of stem orientational distribution, density of stems, stem dielectric constant, canopy thickness, rms surface roughness height, fraction of sand and clay components of soil, and soil bulk density.

The same gridded plate used for determining soil surface roughness characteristics has also been used to estimate vegetation characteristics of non-bare fields. In the case of row structure (ie. winter wheat or maize) photographs are taken both along and across the rows, allowing determination of row distance, distance in the row, plant density (number of plants per m²) and plant height. For pasture fields, only grass height is derived from the slides.

Backscattering from a layer of vegetation has been theoretically modelled in different ways. Attema and Ulaby (1978) have represented the vegetation layer by a cloud of spherical water droplets, in order to compute the volume scattering from the vegetation. This same technique has been applied by Hoekman *et al.* (1982) in a multi-layer vegetation model. The approach produces a relatively simple model with few parameters, but the parameters are not easily related to any measurable vegetation characteristics (Troch *et al.*, 1999).

Lang (1981) and Lang and Sidhu (1983) have modelled the backscattering coefficient from a vegetation canopy by a layer of discrete scatterers over a flat lossy ground. The discrete scatterers in this case were the leaves, which were represented by lossy circular dielectric discs that were small in comparison to the wavelength, having prescribed orientation statistics. The distorted Born approximation, which is applicable when the leaves have small albedo (Lang, 1981), was then used to compute the backscattered power from the vegetation (σ_{veg}^o) by

$$\sigma_{veg}^o = \sigma_d^o + \sigma_{dr}^o + \sigma_r^o \quad (2.69).$$

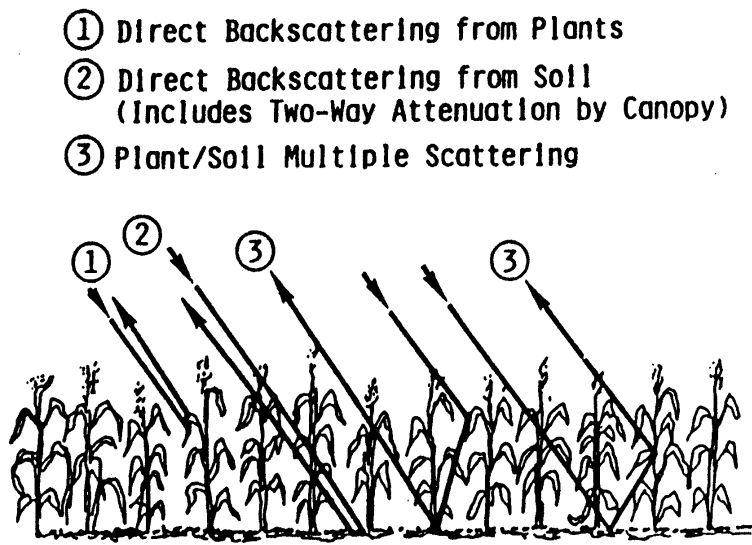


Figure 2.21: Schematic illustration of backscattering mechanisms from a vegetated surface (Ulaby *et al.*, 1996).

The direct backscattering contribution σ_d^o represents the incoming wave that propagates into the vegetation and is scattered directly back to the observer. The direct reflected term σ_{dr}^o results from two different but similar mechanisms. In one case, the wave is scattered and then reflected from the ground towards the observer, whereas in the second case, the wave is first reflected from the ground interface and then scattered towards the observer. The reflected scattering term σ_r^o represents the sum of all waves that are first reflected from the ground, then scattered, and finally again reflected by the ground towards the observer. A schematic illustration of these backscattering mechanisms is given in Figure 2.21. For vegetation with an above ground biomass less than 0.5 kg m^{-2} , the σ_{dr}^o and σ_r^o are negligibly small and the transmissivity of the vegetation approaches one. Therefore, under this condition the effect of vegetation cover may be ignored (Ulaby *et al.*, 1996). The full equations for this modelling approach are summarised in Troch *et al.* (1999).

Troch *et al.* (1999) have presented a theoretical model for the total backscattering coefficient from a soil-vegetation layer (σ_{total}^o), by combining the bare soil backscattering coefficient (σ_{bare}^o) from the IEM (2.46) with the vegetation backscattering coefficient (σ_{veg}^o) from (2.69) by

$$\sigma_{total}^o = \sigma_{veg}^o + \sigma_{ground}^o \quad (2.70),$$

where

$$\sigma_{ground}^o = \Gamma_{veg}^2 \sigma_{bare}^o \quad (2.71)$$

$$\Gamma_{veg}^2 = \exp(-4 \operatorname{Im}(k_v) d_{veg}) \quad (2.72),$$

and σ_{ground}^o is the backscattering from the ground covered with vegetation, Γ_{veg} represents the two-way attenuation by the vegetation, d_{veg} is the vegetation height (cm), $\operatorname{Im}(\)$ is the imaginary component, and k_v is a propagation constant which depends on the dielectric properties of the vegetation layer and the incidence angle.

Due to the complexity of theoretical soil-vegetation backscattering models, Lin *et al.* (1994b) have developed an empirical backscattering model for grass-covered areas from a combination of experimental and simulated data. By including only the most sensitive soil-vegetation parameters in the regression model, the following relationships were obtained.

$$\begin{aligned} (\sigma_{hh}^o)^{-0.21} = & 22.27952 + 0.00009502(\vartheta)^{2.39} - 19.67739(\epsilon_{veg})^{0.01} \\ & - 0.1959691 \left(\frac{d_{veg}}{100} \right)^{1.07} - 0.2731618 \log(\theta \times 100) \end{aligned} \quad (2.73a)$$

$$\begin{aligned} (\sigma_{vv}^o)^{-0.11} = & 2.48103 + 0.00000157(\vartheta)^{2.93} + 0.0001202(\epsilon_{veg})^{1.73} \\ & - 0.3203591(\rho_b)^{0.39} + 0.2320771(S \times 100)^{1.07} \\ & - 0.8883097(\theta \times 100)^{0.42} \end{aligned} \quad (2.73b)$$

where ϑ is the incidence angle (degrees), d_{veg} is the vegetation height (cm), θ is the volumetric soil moisture fraction, S is the sand mass fraction of the soil, ρ_b is the soil bulk density (g cm^{-3}) and ϵ_{veg} is the vegetation dielectric constant, which can be estimated by a relationship with volumetric water content given by Ulaby and El-Rayes (1987).

To quantitatively estimate the effect of a vegetation layer on backscattering under ERS and JERS satellite configurations, Troch *et al.* (1999) undertook a simulation study, which compared the backscattering coefficient estimated for bare soil from the IEM (2.46), with that from a vegetated soil using (2.70). The results of this study showed that soil moisture measurement over grass-covered areas using ERS (C-Band) should be possible without explicitly accounting for vegetation characteristics when the grass height is less than 25 cm and the vegetation volumetric water content is less than 70%. It was also shown that grassland is basically transparent when using JERS (L-Band), even at vegetation heights greater than 60 cm. However, Sano *et al.* (1998) suggest that the contribution of backscattering from vegetation may not be negligible in semi-arid regions, because of the typically low soil moisture contents.

2.4.5.7 Topographic Effects

Because of the high spatial resolution of SAR data, surface topography must often be accounted for. In addition to fore-shortening and layover effects (Engman, 1991), topography affects the soil moisture inference from backscattering observations in two ways. First, if the topography is not taken into account during the SAR data calibration, this can cause large absolute and relative calibration errors (van Zyl *et al.*, 1993). Second, the topography causes the local incidence angle to be different from that assumed for a flat surface (van Zyl, 1993). The cumulative effect is that the algorithm under-estimates the soil moisture content and over-estimates the surface roughness for surfaces tilted towards the radar, while it under-estimates the roughness and over-estimates the soil moisture for surfaces tilted away from the radar (Dubois *et al.*, 1995b). The *hh* polarised signals appear to be most sensitive to the topographic effect (Lin *et al.*, 1994b).

During normal SAR processing, a flat earth is assumed when performing radiometric corrections such as antenna pattern removal and scattering area removal. The effect of a sloping terrain is to cause the actual scattering area to be different from that calculated using the flat earth assumption. Van Zyl *et al.* (1993) have shown that this effect, which is present for both airborne and spaceborne SAR data, may easily cause calibration errors larger than 1 dB. The

effect of ignoring topography during antenna pattern removal has been shown to introduce errors of several decibels in the case of airborne systems, while being negligible for spaceborne. For moderate relief areas, van Zyl *et al.* (1993) have shown that scattering area removal leads to errors that are smaller than 1 dB in most of the image, while for high relief areas there may be errors on the order of 5 dB or more for the leading slopes.

Variations in slope and aspect cause variations in the incidence angle that affect the magnitude of the returned signal, resulting in a non-uniform response of the soil to microwave illumination. Furthermore, significant variations in topography make georeferencing of the radar imagery extremely complicated. To minimise the effects of topography on the backscattering, it has been suggested that if possible, the direction of the radar illumination be aligned with the valley direction, thus reducing the deviation in local incidence angle (Giacomelli *et al.*, 1995).

The local incidence angle of each individual pixel may be calculated using the geometry of the remote sensing system and topographic information from a **Digital Elevation Model (DEM)** by the expression (Robinson, 1966)

$$\cos \vartheta = \cos S \cdot \cos Z + \sin S \cdot \sin Z \cdot \cos(T - A) \quad (2.74),$$

where ϑ is the local incidence angle (degrees), S is the slope of the pixel (degrees), Z is the zenith angle (degrees) of the remote sensing system defined as the angle between the radar and the normal to the horizontal surface at that position, T is the actual flight track of the remote sensing system (degrees), and A is the aspect angle of the pixel position (degrees). T and A are defined to be zero to the north and increase counter clockwise.

2.4.5.8 Saturation and Frost Effects

Mérot *et al.* (1994) and Altese *et al.* (1996) have shown that radar data are ambiguous when ponding conditions occur, due to the contradictory influence of the dielectric effect and the specular effect on the backscattering coefficient. It has also been suggested by Gineste and Mérot (1995) that the radar signal starts to decrease before saturation, which is in keeping with the prediction of theoretical

models that a saturation of the signal owing to a saturation of the soil dielectric constant occurs at high soil moisture content (Autret *et al.*, 1989). Mérot *et al.* (1994) have also found that backscattering values are significantly decreased when frost occurs, due to the low dielectric constant of ice.

2.4.6 REMOTE SENSING OBSERVATION DEPTH

The depth of soil over which the soil moisture can be inferred from remote sensing observations, known as the observation depth, is important for application of these measurements. However, there is little quantitative research in the literature on observation depth, particularly for visible and infra-red. It has been reported however, that correlations have been found for soil moisture content in the upper few millimetres of soil with visible and infra-red observations (Idso *et al.*, 1975; Sadeghi *et al.*, 1984).

Estimation of the observation depth for passive microwave observations appears to have received more attention than any other type of observation. D'Urso *et al.* (1994) have described the microwave response from soil as the result of the integration over a profile, with the importance of each depth decreasing as one moves towards the deeper layers.

On the basis of both experimental (Newton *et al.*, 1982; Newton *et al.*, 1983; Raju *et al.*, 1995) and theoretical work (Wilheit, 1978; Schmugge and Choudbury, 1981; Ulaby *et al.*, 1986), it is believed that the thickness of the near-surface soil layer that can effect such a response in a significant way for passive microwave remote sensing is between one-tenth and one-quarter of a wavelength. Although there is little quantitative evidence in the literature, it is believed that the thickness of this layer is approximately the same for both active and passive microwave remote sensing (Schmugge 1985; Engman and Chauhan, 1995; van Oevelen, 1998). Therefore, by increasing the sensors wavelength it would appear possible to investigate a thicker layer of soil. However, there is currently an upper limit on the wavelength that may be used due to radio frequency interference at wavelengths beyond L-Band (Jackson, 1980; Jackson, 1993; D'Urso *et al.*, 1994; Giacomelli *et al.*, 1995).

Although observation depth is usually only discussed in relation to wavelength, the depth of soil over which microwave instruments are sensitive is also dependent on the soil moisture content. As the soil moisture content is increased, the observation depth decreases (Njoku and Kong, 1977; Newton *et al.*, 1982; Arya *et al.*, 1983; Bruckler *et al.*, 1988; Engman and Chauhan, 1995; Raju *et al.*, 1995). Furthermore, Bruckler and Witono (1989) found that their radar responded to a depth of approximately 1 cm for wet soils, and approximately 5 cm for dry soils. The observation depth is also noted to be a function of incidence angle, wave polarisation, surface roughness and vegetation cover (Arya *et al.*, 1983) and soil moisture profile shape (Njoku and Entekhabi, 1996).

2.5 CHAPTER SUMMARY

This chapter has reviewed the methods commonly used for measuring soil moisture content over the soil profile at specific locations. In addition, the measurement of near-surface soil moisture content from remote sensing observations has been reviewed, along with the most appropriate remote sensing instruments and satellites currently available for soil moisture studies.

It has been found that of the remote sensing observations used for measuring the near-surface soil moisture content, microwave observations have the greatest utility, as a result of their all weather capabilities. Moreover, active microwave observations have the greatest utility for application to agriculture and hydrologic studies, as a result of their high spatial resolution and availability of operationally collected data.

However, active microwave data is more sensitive to surface roughness, vegetation and topographic influences than the passive microwave data. Furthermore, the interpretation of microwave data (passive and active), is dependent on the relationship between dielectric constant and volumetric soil moisture content, which has been shown to be heavily dependent on the near-surface soil temperature. Hence, the interpretation of active microwave remote sensing data requires knowledge of the soil temperature.